# NEW PARTICLE FORMATION IN AN AGRICULTURAL ENVIRONMENT

---

MASTER'S DEGREE REPORT

CHEMISTRY

*Specialty:* ENVIRONMENTAL SCIENCES AND ENGINEERING

Defended publicly
On September 18th, 2019
At the University of Angers

By Leïla SIMON

---

Internship location: Laboratoire des Sciences du Climat et de l'Environnement, Orme des Merisiers, 91191 Gif-sur-Yvette
Supervisors: Jean-Eudes PETIT, Researcher; Julien KAMMER, Post-Doctoral researcher

University supervisor: Maxime PONTIE, University Professor

# NEW PARTICLE FORMATION IN AN AGRICULTURAL ENVIRONMENT

---

MASTER'S DEGREE REPORT

CHEMISTRY

*Specialty:* ENVIRONMENTAL SCIENCES AND ENGINEERING

Defended publicly
On September 18th, 2019
At the University of Angers

By Leïla SIMON

---

Internship location: Laboratoire des Sciences du Climat et de l'Environnement, Orme des Merisiers, 91191 Gif-sur-Yvette
Supervisors: Jean-Eudes PETIT, Researcher; Julien KAMMER, Post-Doctoral researcher

University supervisor: Maxime PONTIE, University Professor

université angers

## ENGAGEMENT DE NON PLAGIAT

Je, soussigné (e) Leila SITON,

déclare être pleinement conscient(e) que le plagiat de documents ou d'une partie d'un document publiés sur toutes formes de support, y compris l'internet, constitue une violation des droits d'auteur ainsi qu'une fraude caractérisée. En conséquence, je m'engage à citer toutes les sources que j'ai utilisées pour écrire ce rapport ou mémoire.

Signature :

MASTER'S DEGREEE
Chemistry
Specialty : « **Environmental Sciences and Engineering** »

| | |
|---|---|
| YEAR: 2017-2019 | PRESENTATION DATE: September, 18th, 2019 |
| AUTHOR: Leïla SIMON | INTERNSHIP LOCATION: LSCE |
| UNIVERSITY SUPERVISOR: Maxime PONTIE | COMPANY SUPERVISOR: Jean-Eudes PETIT |

TITLE:
NEW PARTICLE FORMATION IN AN AGRICULTURAL ENVIRONMENT

KEYWORDS: New Particle Formation, agriculture, atmospheric aerosols, nucleation, growth

ABSTRACT:

The understanding of sources and formation mechanisms of particulate pollution represents a major challenge on both scientific and social levels, through sanitary and climatic impacts. The Ile-de-France region is particularly affected by episodes of particulate pollution which are often related, during spring, to agricultural activities. However, while primary emissions are quite well documented, the agricultural ecosystem is still scarcely studied in terms of new particle formation (NPF). This process corresponds to the formation of a particulate nucleus followed by their growth, by gas-particle conversion of semi-volatile compounds. While NPF has already been observed in numerous locations, very few studies were conducted in the agricultural field.

As part of the ADEME-AgriMultiPol project, a field campaign took place on the FR-Gri ICOS site in the Grignon experimental farm, from March 13th to May 14th 2018. In order to identify new particle formation events, measurements of the particle number size distribution were carried out. Complementary analyses of chemical characterization of the particles, meteorological parameters and gas concentration have been performed to investigate the origin of NPF.

This unique dataset in the vicinity of agricultural activities enabled firstly to identify diurnal and nocturnal new particle formation events. Secondly, linking the events with the environmental parameters highlighted conditions and interesting tendencies. It was shown that the diurnal events could be linked to the photooxidation of precursor VOCs, while the nocturnal events seemed to be favoured by the presence of nitrogen dioxide and ammonia.

Finally, a comparison with measurements at the SIRTA station, 27 km away, showed that these events occurred on a regional scale, as they happened almost simultaneously at both sites.

RESUME:

La compréhension des sources et des mécanismes de formation de la pollution particulaire représente un enjeu majeur aux niveaux scientifique et sociétal, au travers d'impacts sanitaires et climatiques. L'Ile de France est particulièrement touchée par des épisodes de pollution particulaire auxquels, au printemps, l'agriculture est souvent associée. Pourtant, alors que les émissions primaires sont de mieux en mieux documentées, l'écosystème agricole reste assez peu étudié au regard de la formation de nouvelles particules (NPF). Ce processus correspond à la formation d'un noyau particulaire suivi d'un grossissement, par conversion gaz-particule de composés semi-volatils. S'il a déjà été mis en évidence dans de nombreuses localisations, il n'existe que très peu d'études en milieu agricole.

Dans le cadre du projet AgriMultiPol, une campagne de mesures a été effectuée sur le site FR-Gri ICOS à la ferme expérimentale de Grignon, sur la période du 13 mars au 14 mai 2018. Afin d'identifier des épisodes de formation de nouvelles particules, des mesures de distribution granulométrique des particules ont été effectuées. Des mesures complémentaires de caractérisation chimique des particules, paramètres météorologiques et concentration en composés gazeux ont été mises en place pour étudier l'origine des NPF.

Ce jeu de données en proximité agricole, unique en son genre, a permis dans un premier temps de mettre en évidence des épisodes de formation de nouvelles particules diurnes et nocturnes. Dans un deuxième temps, le croisement des données a rendu possible la mise en relation de ces épisodes avec les conditions environnementales du site. Il a notamment été montré que les épisodes diurnes pouvaient être liés à la photooxidation de COVs précurseurs, tandis que les épisodes nocturnes semblent être favorisés par la présence de dioxyde d'azote et d'ammoniac.

Enfin, une comparaison avec les mesures effectuées à la station du SIRTA, située à 27 km de Grignon, montre que ces processus se déroulent à l'échelle régionale, car ils ont lieu de manière quasi simultané sur les deux sites.

Je soussigné Jean-Eudes PETIT maître de stage professionnel de Leïla SIMON,
AUTORISE ~~ou N'AUTORISE PAS~~ (1) : la publication des sources bibliographiques, des résumés français, anglais
AUTORISE ~~ou N'AUTORISE PAS~~ (1) : le dépôt du mémoire dans une bibliothèque
Date : 02/09/2019 Signature du maître de stage :

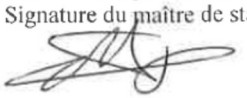

(1) rayer la mention inutile

# Acknowledgements

First of all, I would like to thank Valérie GROS for giving me the opportunity to work in this research team and to go further than the subject of my internship.

I want to thank a lot my supervisors: Jean-Eudes PETIT, for letting me do a bit of experimental, for his teaching, his advices, and his trust; Julien KAMMER, for sharing some of his knowledge on NPF with me, and for taking the time to explain to me how the PTR-ToF-MS works, I'll be able to use it on my own for the next 3 years.

I would like to thank the other interns, Nathan PICOIS (with you every day is Friday), Dini SAAMEH, Emilie HARAN, Florian BERTIN for the great times that we shared. I thank the PhD students (in their 3rd year), Sandy BSAIBES and Baptiste LANGUILLE, for the great conversations, and for making me doubt my choice…

Many thanks to the other members of the CEA team, Christophe BOISSARD, Virgile BERSON, François TRUONG, François DULAC, Dominique BAISNEE, Nicolas BONNAIRE, for their advices on my oral presentations.

I also want to thank my university supervisor, Maxime PONTIE, for reading this manuscript, as well as my jury members, Pierre FRERE and Alain JADAS-HECART.

A special thanks goes to Mélissa MEYER, Axelle MERIEN, Alice FRAYARD, Amandine DRONNE, Amélie COUE, Bérengère LEVIONNOIS, Laureline VALLEE, and Thomas LIMOSIN for these unforgettable 2 years of Master together.

Finally, I would like to thank DIM Qi² for the financial support, enabling the achievement of this internship.

# Table of contents

# List of figures

# List of tables

# List of abbreviations

| | |
|---|---|
| **BL** | Boundary Layer |
| **CCN** | Cloud Condensation Nuclei |
| **CS** | Condensation Sink |
| **EC** | Elemental Carbon |
| **GR** | Growth Rate |
| **J** | Nucleation Rate |
| **NMHC** | Non-Methane Hydrocarbons |
| **NPF** | New Particle Formation |
| **OC** | Organic Carbon |
| **OM** | Organic Matter |
| **PM** | Particulate Matter |
| **PTR-ToF-MS** | Proton Transfer Reaction Time of Flight Mass Spectrometer |
| **RH** | Relative Humidity |
| **SIRTA** | Instrumental Site of Research by Atmospheric Teledetection (Site Instrumental de Recherche par Télédétection Atmosphérique) |
| **SMPS** | Scanning Mobility Particle Sizer |
| **TSP** | Total Suspended Particles |
| **VOC** | Volatile Organic Compound |

# Glossary

**Aerosol**: liquid or solid particle in suspension in the air

**Cluster**: agglomeration of 2/3 molecules

**Condensation**: uptake of low volatility gaseous molecules on particles

**Condensation sink**: variable to determine how fast low volatility molecules condense onto pre-existing aerosols

**Coagulation**: uptake of clusters on particles

**Coagulation sink**: variable to determine how fast fresh nucleated particles are lost through coagulation onto other particles

**Growth**: increase of the diameter of newly formed particles, via nucleation

**Growth rate**: variable to determine the increase of particles mean diameter per time

**New particle formation**: process through which new ultrafine particles are created, characterized by a nucleation and a growth phase

**Nucleation**: gas-phase conversion of semi-gaseous species

**Nucleation rate**: variable to determine the number of nucleation clusters are formed by gas-particle conversion

**Particle number size distribution**: number of particles per volume for each measured diameter ($cm^{-3}$)

**Pollution event**: Time period when pollutants concentration exceeds a threshold

# Introduction

Climate change is one of the most important issues of our time. To this respect, anthropogenic activities play a central role through their impact on the chemical composition of the atmosphere. In particular, the troposphere, the layer of the atmosphere which we live in, is a true chemical reactor. Indeed, reactive gases and particles are mixed under the effect of turbulence, react together, and may form secondary pollutants, whose processes are not comprehensively understood yet.

Megacities, such as Paris (France), are regularly impacted by such kind of pollution, especially during Spring. Although agriculture is often pointed out due to the concomitance with nitrogen-containing fertilizer spreading, the role of the agricultural ecosystem is not clearly defined, especially regarding the formation of secondary pollutants.

It is thus essential to study pollutants emitted by anthropogenic sources such as industries or agriculture, as well as their fate in the atmosphere, in particular their ability to form secondary particulate pollution.

In this context, the scope of this internship is to contribute to the understanding of secondary aerosol formation processes in the vicinity of agricultural activities, in order to better characterize the impact of this source on these processes.

The first chapter of this manuscript presents the laboratory where I carried out my internship, Chapter 2 summarizes current knowledge on this topic, essential to understand the issue and scope of my internship, presented in Chapter 3. The fourth chapter describes the materials used to obtain the dataset, as well as the methodology developed and applied for its analysis. The last chapter presents and discusses the results.

# Chapter 1: Presentation of the laboratory

## I. The Laboratory for Sciences of Climate and Environment

The LSCE, standing for Laboratory for Sciences of Climate and Environment, is a mixed research unit between the CEA (French Alternative Energies and Atomic Energy Commission), the CNRS (French scientific research centre) and the University of Versailles Saint-Quentin-en-Yvelines. It was created in 1988.

CEA is composed of 9 centres throughout France. They are important for French research in fields like energy, life and health sciences, social sciences, and environmental sciences. It is divided in 4 operational directions: Direction of nuclear energy, Direction of military application, Direction of technological research and Direction of fundamental research.

CNRS is a public institution for science and technology, and was created in 1939. The current head of CNRS is Antoine Petit. This entity, one of the most important in the world, is placed under the guardianship of the French Ministry of Higher Education, and possesses more than 1100 laboratories in France.

About 300 researchers, engineers and administrative people work at LSCE, about half of them are permanent and several tens are PhD students. LSCE is part of the Institute Pierre Simon Laplace (IPSL), which regroups actors of research on climate evolution, greenhouse effect, the ozone layer, and processes of environment transformation in planets composing the solar system.

LSCE is also a contributor to IPCC (Intergovernmental Panel on Climate Change), through both the coordination of work package and the writing/reviewing of reports.

## II. Research themes and teams

The laboratory is composed of 3 main research themes, divided in various research groups. The themes are Archives and tracers, Biochemical cycles and transfers in the environment, and Climate and cycles.

- Archives and tracers: The scope of the research groups working in this theme is to understand the dynamic and natural variability of climate and to evaluate the sensitivity of marine and continental ecosystems to climate and anthropogenic changes. One of the activities on which the team focus is the measurement of interactions between atmosphere, oceans, ice, and continents. This theme is composed of 5 teams (CLIMAG, GEOTRAC, GLACCIOS, PALEOCEAN, LANDER)

- Biochemical cycles and transfers in the environment: This department focuses its work on the characterisation and quantification of biogeochemical cycles of greenhouse gases, as well as matter transfers in the environment. This LSCE specialty is divided in 2 axes: the atmospheric approach, and the matter exchanges and lateral transfers on continental surfaces. The teams regrouped here are: ICOS-RAMCES, SATINV, CAE, MOSAIC, GEDI, HYDRO.

- Climate and cycles: This theme uses mostly modelling, one of the lead specialties of LSCE. The research axis is directed on interactions between climate and cycles in multiple time scales. These modelling works are mainly based on the expertise of the observation teams present in LSCE, on one hand for the reconstruction of past climates, and on the other hand for the follow-up of the atmosphere's composition and the fluxes at the interface between atmosphere and surfaces. This theme regroups 4 teams (MERMAID, CLIM, CALCULS, ESTIMR).

## III. The CAE team

The team which I belonged to during this internship is called CAE (Experimental Atmospheric Chemistry) and is part of the second theme (Biochemical cycles and transfers in the environment). The CAE team aims at studying reactive gaseous and particulate species which can potentially impact air quality, ecosystems, and more generally climate. The team aims at characterizing and quantifying the sources, properties and physicochemical transformations of these species.

For this purpose, long-term measurements are carried out at the SIRTA station in order to widely cover the background in the Ile de France region in terms of gases and aerosol concentrations. The team also coordinates and participates in numerous multi-instrumented field campaigns in various environments which are relevant for the understanding of atmospheric chemistry.

# Chapter 2: Scientific background

## I. Generalities

Pollutants in the atmosphere, present in diverse states (gas, liquid, solid), are directly emitted from various sources (natural, anthropogenic) or result from chemical reactions within the atmosphere. Pollutants that are directly emitted are called primary pollutants, and the ones resulting from in-situ transformations are called secondary pollutants.

The main atmospheric pollutants are presented in Table 1:

*Table 1: Main atmospheric pollutants, their state and their main source*

| | **Pollutant** | **Source** |
|---|---|---|
| **Gaseous pollutants** | Volatile Organic Compound (VOC) | Biosphere and anthropogenic |
| | Non-Methane Hydrocarbon (NMHC) | Traffic |
| | VOC-Sulphur | Oceans |
| | Sulphur dioxide ($SO_2$) | Volcanos |
| | Nitrogen oxides (NOx) | Traffic, heating |
| | Ammonia ($NH_3$)/amines | Agriculture |
| **Primary particulate pollutants** | Sea salts | Oceans |
| | Dust | Natural (earth) |
| | Elementary carbon (EC) | Anthropogenic |
| | Organic matter (OM) | Natural and anthropogenic |
| | Metals | Industries |

Atmospheric particles can be classified according to several parameters: their size, their chemical composition, or their origin.

Particle sources could be both natural and anthropogenic (Table 1). Main natural sources are the biosphere (trees and plants), oceans, earth, and volcanos. The anthropogenic sources are traffic (road, maritime, aerial), agriculture, industries, residential wood burning. The sources vary seasonally and so does the contribution of each to the total particle concentration.

Aerosol corresponds to solid or liquid particles in suspension in the air, and is composed of an organic and an inorganic phase. The inorganic phase is composed of metals, sea salts, sulphated compounds, and nitrates. Sulphated aerosols are formed via the oxidation of $SO_2$, which can be either directly emitted in the atmosphere (volcanism, fossil fuels combustion…) or to a lesser extent produced by the oxidation of sulphuric compounds, like dimethylsulfide (emitted by phytoplanktonic activities). Nitrates mainly result from $NO_x$ oxidation (emitted by traffic and biological soil activity) into nitric acid ($HNO_3$), which can further react with gaseous ammonia to form particulate ammonium nitrate. (Brégonzio, 2013)

The carbonaceous fraction is composed of elemental carbon (EC) and organic carbon (OC). EC is emitted from combustion processes, such as traffic or biomass burning, and has a primary

origin. On the other hand, OC is much more complex. It can be directly emitted from a large variety of sources or result from gas-particle conversion of low vapour pressure products, resulting from the gas-phase oxidation of e.g. hydrocarbons (Pandis et al., 1992).

Secondary aerosols can be products of the conversion of gas-phase inorganic or organic precursors into particle phase products, or of the condensation of gaseous species on existing particles. Depending on the precursors, the particulate products are referred to as Secondary Inorganic (SIA) or Secondary Organic Aerosols (SOA) (Nøjgaard et al., 2012).

The main inorganic precursors are ammonium, nitrate and sulphate; while organic precursors include various families of compounds.

SOA contribute to a significant fraction of fine particulate matter that can be as high as 50-80% in polluted regions (Ng et al., 2006). However, because they are formed in situ, determining the origin of secondary particles is arduous.

Characterizing the size of particles in a coherent way may be challenging because they can have different shapes (from cubic to spherical or agglomerates). That is why different types of particle diameters are defined:

- Aerodynamic diameter ($D_a$): the diameter of the aerodynamic equivalent of a sphere with a density of 1000 $kg.m^3$, that has the same settling velocity as the particle of interest.
- Mobility diameter ($D_m$): the capacity of a particle to follow an air flow will depend on its mobility diameter. Bigger particles will impact on an obstacle put in their way while smaller ones will follow the air flow around the obstacle.
- Electrical mobility diameter ($D_{em}$): the deviation of a charged particle induced by an electrical field will depend on its electrical mobility diameter.

The aerodynamic diameter is commonly used to classify particulate matter. For example, $PM_{10}$ corresponds to particulate matter with an aerodynamic diameter smaller than 10 µm (Table 2). Different particle modes are defined according to their diameter by Dal Maso et al. (2005).

*Table 2: Classification of particles depending on their aerodynamic diameter*

| **Mode name** | **Particle class name** | **Diameter** |
|---|---|---|
| | Total suspended particles (TSB) | All particles |
| | $PM_{10}$ | < 10 µm |
| Coarse | | 2.5-10 µm |
| Fine | $PM_{2.5}$ | < 2.5 µm |
| Ultrafine | $PM_{0.1}$ | < 100 nm |
| Aitken | | 25-100 nm |
| Nucleation | | < 25 nm |

# II. Impacts

Depending on their size and composition, particles have different impacts on air quality, health and climate.

## 1) Impacts on air quality

The impact of aerosol on human health is induced by their ability to enter the human body through the respiratory system (Figure 1). The smaller the particles, the deeper they can go into the organism. While, for example, nose and lungs can hold coarse particles, the fine and ultrafine ones can flow through the lungs and the finest fraction can even reach the cardiovascular system. Aerosol is composed of various elements that will have toxic effects on the organism, and the presence of diverse compounds is responsible for cocktail effects, whose impact is difficult to quantify (Uzu et al., 2019).

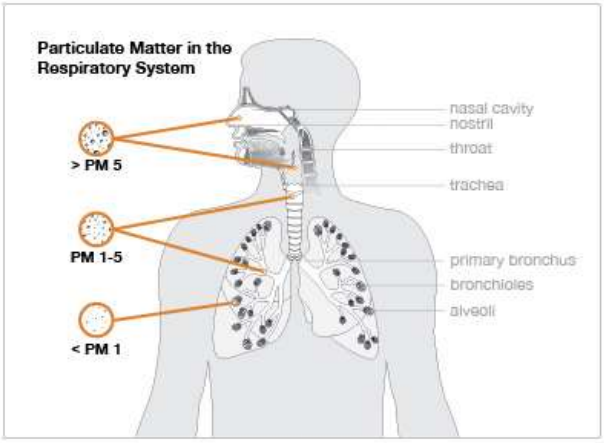


*Figure 1: Particulate matter in the respiratory system (pharco.co.uk)*

## 2) Impacts on climate

Depending on their composition, particles have different interactions with solar light, which lead to a complex contribution to the Earth's radiative budget (Figure 2). Indeed, while black carbon particles strongly absorb light (positive radiative forcing, i.e. heating impact), other compounds such as nitrate or sulphate scatter light.

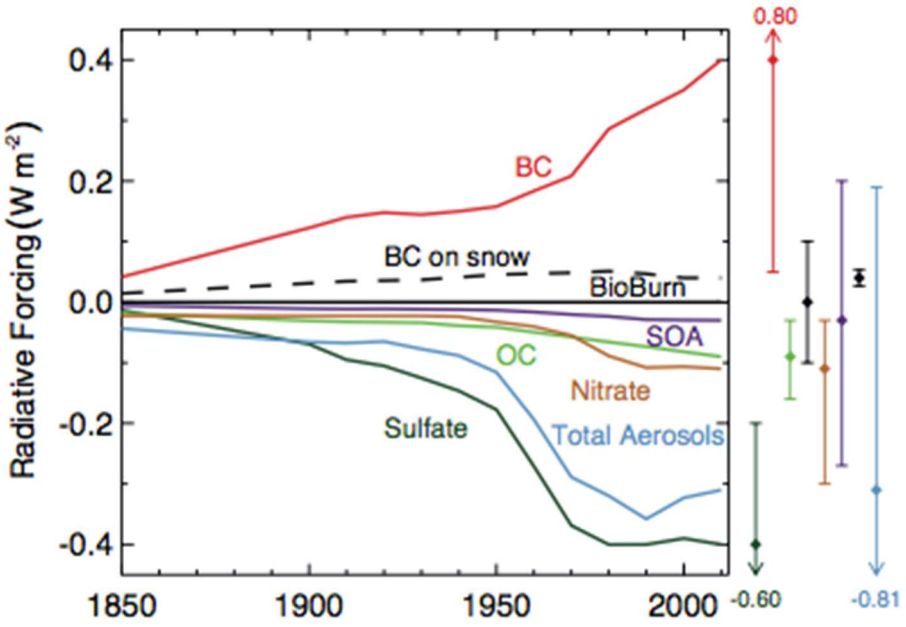


*Figure 2: Radiative forcing of aerosols (adapted from IPCC, 2013)*

However, the interaction of particles with light cannot be summarized to this so-called direct effect. Indeed, Figure 3 gives an overview of the different effects that aerosols may have on climate, through formation of or uptake by clouds.

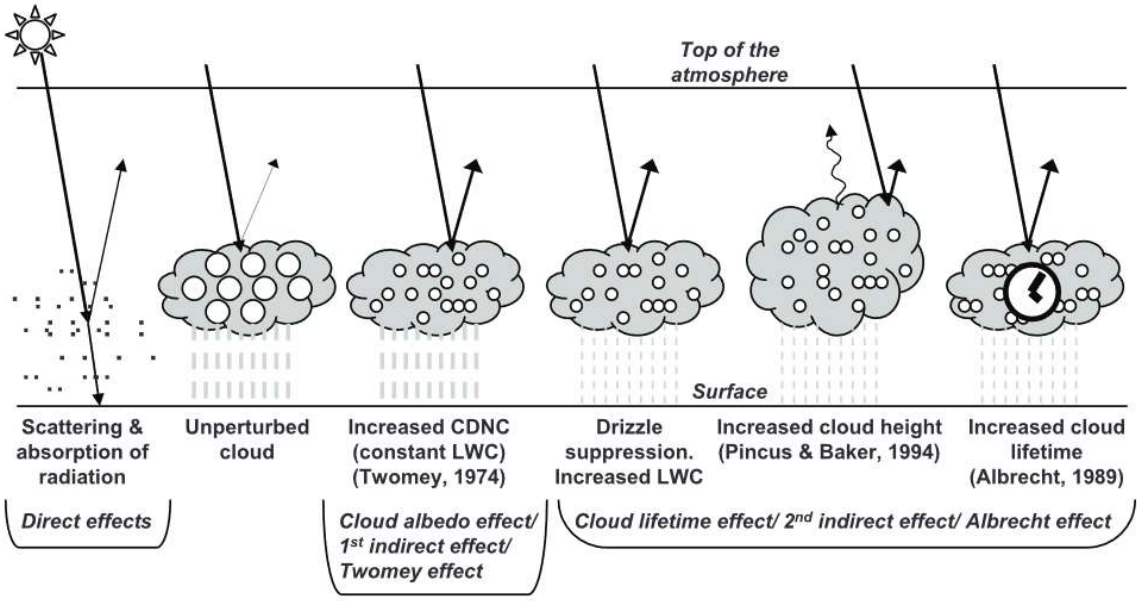


*Figure 3: Direct and indirect effects of aerosols on climate (from IPCC, 2007)*

Aerosols can act as Cloud Condensation Nuclei (CCN), particles on which water vapours may condense and that act as cloud precursors. Moreover, the presence of aerosols in clouds modifies the cloud's albedo, i.e. its ability to reflect light. Then, anthropogenic aerosols, on addition to natural ones, increase CCN number, and finally the number of droplets inside clouds (Figure 3). As a result, cloud height, lifetime and liquid water content increase, finally affecting climate (IPCC, 2007).

It has been shown that about half of the CCN originate from NPF (Merikanto et al., 2009).

# III. New Particle Formation

NPF describes the process through which new ultrafine particles are created in the atmosphere – in opposition to the "old" ones, already present.

The NPF process is characterized by a nucleation phase and a subsequent growth, resulting from condensation and coagulation, as presented in Figure 4. Both phases are detailed hereinafter.

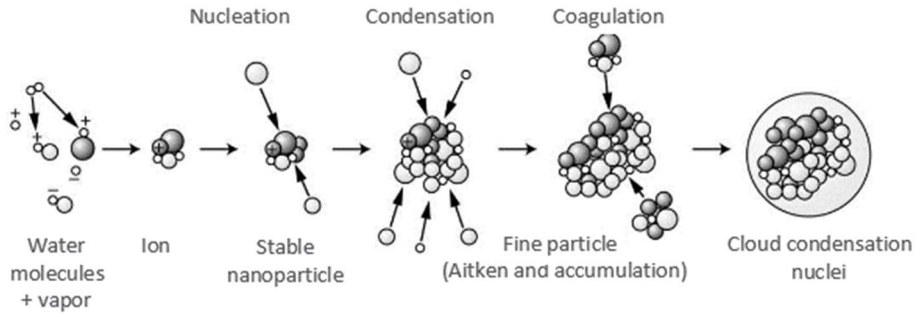


*Figure 4: Process of formation and growth of secondary particles (from Delmas et al, 2005)*

## 1) Nucleation phase

Nucleation corresponds to a gas-particle conversion process of semi-gaseous species via the formation of a particulate nucleus.

In the atmosphere, water condenses when ambient relative humidity reaches 100%. In the same way, gaseous substances might condense when they reach a supersaturation, so that vapour pressure of the gas is higher than its saturation vapour pressure. However, supersaturation alone is not enough to allow nucleation, gaseous precursors must overcome the nucleation barrier. Molecules in a supersaturated state can nucleate but as long as their radius is smaller than the so-called critical cluster radius (corresponding to the point where it is thermodynamically better for the species to stay in the particulate state), the molecules in the cluster will preferably dissociate to go back to gaseous phase. As a result, NPF might happen when gaseous molecules concentration is high enough to create nuclei that will be big enough to persist in the environment (Kulmala, 2003; Seinfeld and Pandis, 2006; Curtius, 2009).

Another important condition required for nucleation to happen is that the molecules form clusters – particulate nuclei – faster than they condense onto pre-existing aerosols. In fact, it is energetically more favourable for gas molecules to condense on particles already existing than forming new ones. But if there are not enough particles for gaseous molecules to condense to, or if the concentration of these substances is high, nucleation can be favoured.

The main compound involved in this process is sulphuric acid, formed via the oxidation by hydroxyl radical (OH) of sulphur dioxide (Seinfeld and Pandis, 2006). The main and first studied nucleation mechanisms involve binary water-sulphuric acid nucleation via the formation of clusters between $H_2O$ molecules and hydrated $H_2SO_4$ molecules (Seinfeld and Pandis, 2006 (and references)). Other mechanisms that have been brought to light are ternary water-sulphuric-ammonia nucleation and ion-induced nucleation (Kulmala et al., 2004).

## 2) Growth phase

The growth of these clusters formed during the nucleation phase occurs via condensation and coagulation processes.

Condensation is the uptake of low volatility gaseous molecules on particles. Gaseous molecules condense on the newly formed particles and thus enhance their growth into stable ultrafine particles. The substances involved here are generally different than those involved in the nucleation phase. Many studies show that volatile organic compounds (VOCs) can be oxidized by hydroxyl (OH) and nitrate ($NO_3$) radicals, or by ozone ($O_3$), producing less volatile substances – heavier – that will be able to condense (Kroll and Seinfeld, 2008; Gooch, 2011).

The coagulation process is different. The clusters formed during the nucleation phase, instead of growing thanks to other volatile compounds, can coagulate on the surface of newly formed particulate nuclei. This process also depends on the thermodynamic gas-particle equilibrium and leads to the increase of the diameter of the fresh particles.
The coagulation process implies the diminution of the number concentration and the increase of the average aerosol size, without changing its total mass (Brégonzio, 2013).

Thus, the particles are formed at a few nanometers and grow to reach sizes around 50-100 nm. The obtained ultrafine particles are big enough to play the role of Cloud Condensation Nuclei (CCN), with typical size of 50-150 nm. The ability of aerosols to act as CCN depends on their size and chemical composition. A lot of studies show that NPF events are a source of CCN: in the study of Rose et al (2017), 61% of NPF events lead to CCN number concentration increase (Dameto de España et al., 2017; Rose et al., 2017).

The understanding of nucleation and growth processes is thus crucial for the characterization of NPF events and to understand the global behaviour of the aerosol in the atmosphere.

Both nucleation and growth phases composing a NPF event can be illustrated by a contour plot of the measured particle number size distribution as a function of time, as presented in Figure 5.

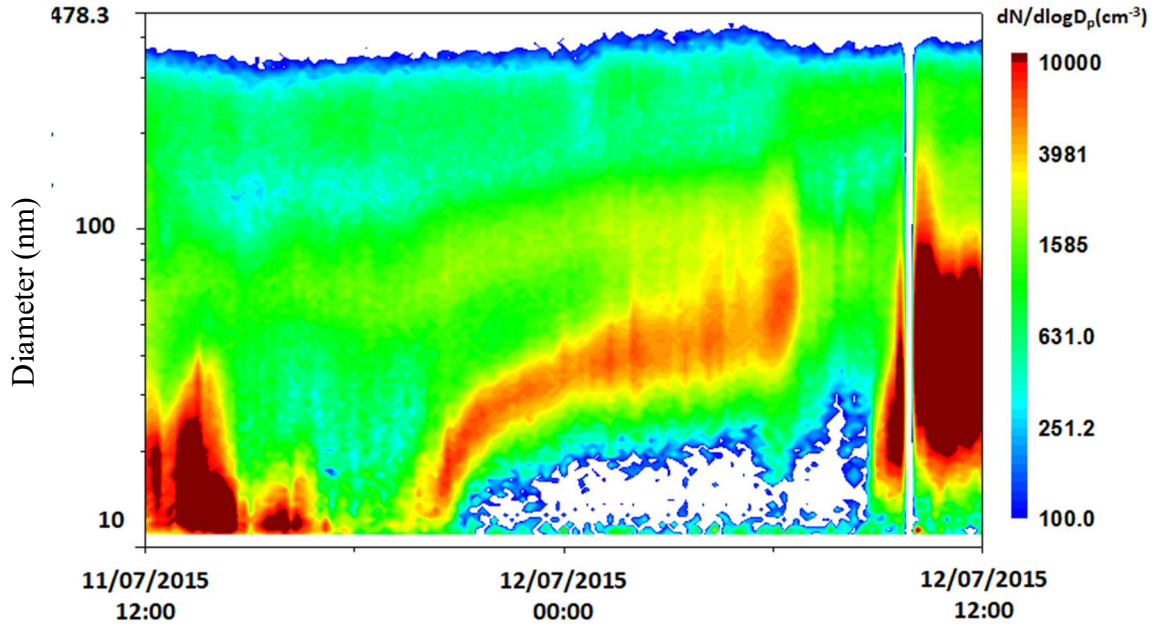


*Figure 5 : Time series of the particle number size distribution, as example of a NPF event (from Kammer et al, 2018)*

The graph is a representation of the particles diameter in log scale (in nm, y axis) as a function of time (as a date, x axis). The colour scale gives the particle number of each diameter per volume (in $cm^3$, also log scale), and fills the graph.

The typical "banana" shape observed on the graph traduces the different steps of the NPF process described previously. There is first a burst of particles at a few nanometers, around 7 PM, corresponding to the nucleation step, where a lot of very small particles are created and are able to persist in the atmosphere. After that, the growth phase corresponds to the increase in the diameter where the concentration is the highest until a plateau.

This picture was taken from the study of Kammer et al. (2018), performed in the French Landes forest, where the environment is clean enough to obtain distinguishable NPF events.

There are other bursts of particles before and after the event but they are not followed by a growth phase. As a result, they do not represent a NPF event.

# Chapter 3: Scope of this internship

NPF events have been observed in various environments (rural, urban, boreal forest, mountains) and in various places of the world (Europe, Arctic, China) (Kulmala et al., 2004; Kerminen et al., 2018). The vast majority of the observed events occurred during daytime, whose process starts to be well documented. However, observations of nighttime NPF have been much more scarcely reported in the literature (Kerminen et al., 2018), mainly in forest environment, or urban and suburban sites in China (Ortega et al., 2012; Kammer et al., 2018; Chen et al., 2019; Gao et al., 2019;).

Moreover, these observations are often carried out in sites with strong biogenic emissions and, in comparison, less studies focused on urban and suburban environments in Europe (Kulmala et al., 2004).

Finally, even though the available literature covers a large range of observations, to my knowledge no study focused on NPF in near agricultural environments. Indeed, agricultural activities play an important role in the formation of secondary pollution (ADEME, 2012), notably through the emission of ammonia, but some processes still remain unclear.

In an attempt to improve our knowledge on NPF, the scope of this internship was to study for the first time NPF events on a mixed periurban-agricultural site, where a measurement campaign was carried out in Spring 2018, as part of the ADEME-AgriMultiPol project.

With the approach used, I tried to answer the following scientific questions:
- Do we observe NPF events in the vicinity of agricultural activities?
- What are the conditions to their occurrence?
- Is there a link between NPF events and agricultural activities?

The strategy applied in my internship consisted first in developing a methodology to highlight these events, by representing the size distribution data as temporal series. Then, I linked the events with meteorological and physico-chemical parameters, in order to find trends that would help to understand the process and conditions of these events. Finally, analysing the gas ($NH_3$, $NO_x$, $O_3$, VOCs) concentrations might allow us to identify precursor gases involved in NPF.

# Chapter 4: Materials and methods

## I. Measurement campaign

### 1) The ICOS FR-Gri site

The field measurement campaign was conducted at the ICOS FR-Gri site situated in Grignon (48°51' N, 1°58' E), 35 km West of the centre of Paris (France) and integrated to the ICOS (Integrated Carbon Observation System) network (Figure 6). The site is a 9-ha field sowed with winter wheat.

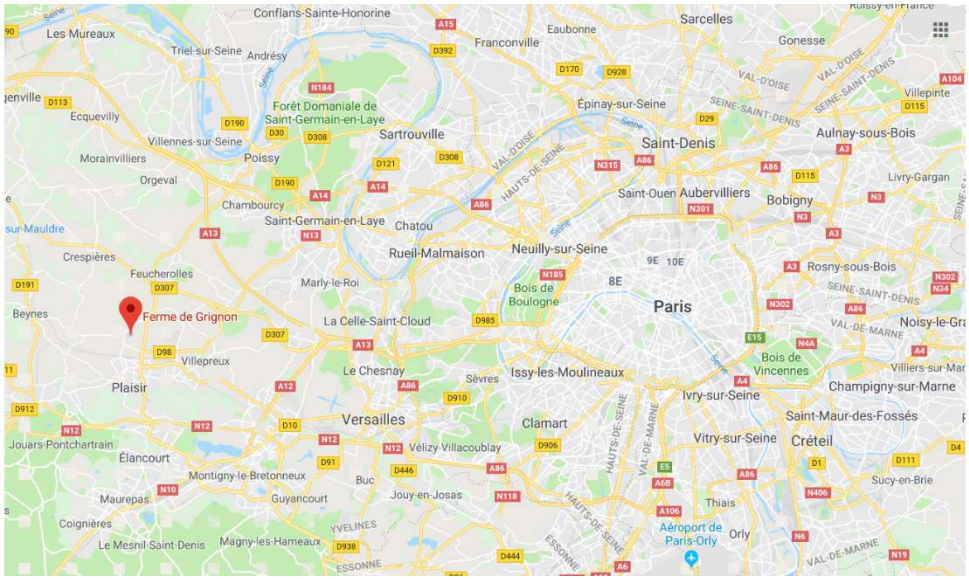


*Figure 6: Location of the measurement site: the Grignon Farm (Google Maps, 2019)*

The field belongs to a farm facility, whose main buildings are located 450 m South-West, with about 200 milky cows, 500 sheep and a production of about 900 lambs. The field is surrounded by other agricultural fields at the south and roads with average traffic in north, east, south and south-west, as can be seen on Figure 7.


*Figure 7: View of the field (circled) where the measurements were carried out (Google Maps, 2019)*

## 2) Particle number size distribution

Particle number size distribution is crucial to identify new particle formation. In this perspective, a Scanning Mobility Particle Sizer (SMPS, TSI model 3080) was used for a period covering March 13$^{th}$ to May 15$^{th}$, 2018. The instrument is composed of three distinct parts: an ionising source (neutralizer), a classifier, and an optical particle counter.

During the experimentation, the instrument was sampling ambient air at a flow of 0.3 L.min$^{-1}$ through conductive silicone tubing (intern diameter of 4.5 mm), placed at 3 m above the ground. The sampled air contains polydispersed particles, whose size range potentially varied from a few nanometers to several tens of micrometers. In order not to clog the instrument, an impactor placed at the inlet of the instrument trapped the biggest particles (of micronic sizes). The particles escaping the impactor were then dragged towards an X-ray ionising source. Close to this source, the particles, that are naturally ionised (positively or negatively), captured charges that counterbalance their natural charge, forming a bipolar distribution at the equilibrium.

An electrostatic classifier (DMA, Differential Mobility Analyzer, TSI model 3082, see Figure 8) then enabled particles separation. The ionized particles penetrated in an electrical field induced by a quadrupole and they were deviated according to their electrical mobility diameter.

The particles were then counted thanks to an optical counter (CPC, Condensation Particle Counter, TSI model 3768, see Figure 9), that measured the light diffused by the particles when they crossed the light ray of a photodiode. The particle size range of the analysed particles covered diameters from 4.61 nm to 156.8 nm.

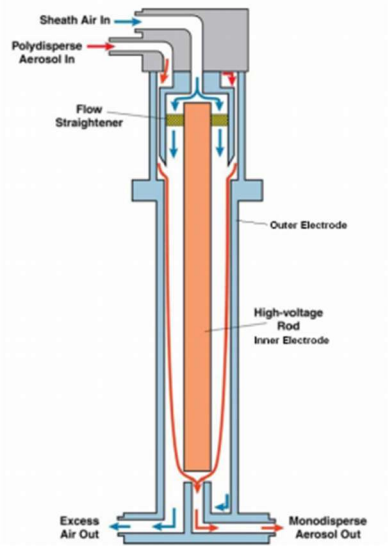


*Figure 9: Schema of a differential mobility analyser (TSI)*

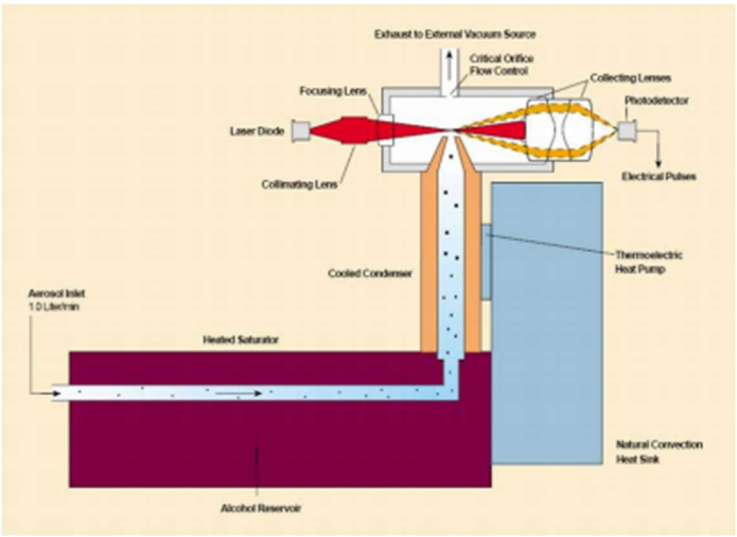


*Figure 8: Schema of a condensation particle counter (TSI)*

The particle losses on the sampling tube walls were evaluated and corrected according to the methodology described by Willeke and Baron (1993). The maximal losses occurred for the finest diameters and were of about 46% according to the experimental configuration (Gros et al., 2019).

### 3) Other measurements useful for the study

At the same time, other measurements were carried out to characterize the meteorological conditions, the chemical composition of the particles, and the concentration of other gaseous compounds in the atmosphere.

For the meteorological conditions, the parameters measured were inter alia the air temperature, the relative humidity, the rain, the solar radiation, and the wind speed and direction.

An Aerosol Chemical Speciation Monitor (ACSM) was used to determine the composition of $PM_1$, i.e. the total mass concentration of particles present, the concentration of organic matter (OM), sulphate ($SO_4^{2-}$), nitrate ($NO_3^-$), chloride ($Cl^-$) and ammonium ($NH_4^+$), in $\mu g/m^3$.

In addition, the concentration of Black Carbon (BC) was measured using an aethalometer AE33 (Magee Scientific), which can separate the fraction of BC coming from fossil fuel ($BC_{ff}$) from the fraction resulting of wood burning ($BC_{wb}$). Ammonia ($NH_3$) was measured using a photoacoustic analyser (LSE monitors). Concentrations of $NO_x$ and ozone were respectively measured with a chemiluminescent analyser (Model 42C, Environment SA) and a UV photometry analyser (Model 49i, Thermo Fischer).

Finally, the concentration of volatile organic compounds (VOCs) was measured by PTR-Qi-ToF-MS (Proton-Transfer-Reaction Quadrupole Time-of-Flight Mass Spectrometry). The PTR-Qi-ToF-MS is a soft ionization technique allowing online, high sensitive measurements of most of the VOCs.

## II. Methodology applied for data analysis

### 1) Identification of NPF events

Identification of NPF from SMPS data requires two steps. First, it was necessary to plot the time series of particle number size distribution over the campaign. In order to do this, I developed a script using the R language (RStudio Team, 2016). This software is widely used in scientific research, as it is a powerful tool for data analysis and statistics.

Since I had no experience in R coding, I had to get familiar with this language. Therefore, a significant part of my internship was dedicated to the development of R scripts. The script corresponding to this step can be found in Appendix 1.

Secondly, a day-by-day visual inspection of the particle number size distribution time series was carried out to identify NPF events.

A NPF event traduced by a “banana shape” means that first a clear increase could be observed on the finest particle mode (nucleation/Aitken mode), followed by a growth during at least 2 hours, as recommended by Dal Maso et al. (2005). Days where it was tricky to discern an event, but its presence could not be excluded were characterized as “unclear”. Thus, all days of the campaign fell into one of the following categories according to the criteria presented in Table 3.

*Table 3: Categories of days and their corresponding criteria*

| **Category** | NPF event | unclear | non event |
|---|---|---|---|
| **Criteria** | Typical shape of NPF, with the presence of particles with a diameter <10 nm (nucleation phase), followed by their growth during at least 2h | Presence of ultrafine particles and growth, but no clear observation of a NPF event | Absence of ultrafine particles or of their subsequent growth |

## 2) Statistical analysis

The separation of particle formation days from days with no formation enabled a statistical study for a deeper understanding of the conditions and the process involved in the events. In fact, linking the obtained categories of days to the corresponding meteorological conditions, particle composition, and gaseous compounds concentration might provide trends for each category. To this end, a statistical analysis consisting of calculating the hourly median value of each parameter as well as its normalized variance was carried out. These values can then be represented as diurnal profiles in order to compare the three categories of days.

This study can give us hints of which parameters might favour the occurrence of NPF events.

## 3) Quantitative study of the NPF events

To characterise the physical properties of a NPF event, nucleation and growth rates are usually calculated (Kulmala et al., 2001; Dal Maso et al., 2005; Xiao et al., 2015).

Since both condensation and coagulation processes contribute to the observed NPF, condensation and coagulation sinks are used to characterize quantitatively the growth step.

### a. Condensation and coagulation sinks

The condensation sink (CS) determines how fast low volatility molecules condense onto pre-existing aerosols.

Equation (1) is used for its calculation (Kulmala et al., 2001):

$$CS = 4\pi D \cdot \sum_i \beta_{m,i} r_i N_i \quad (1)$$

Where

- D is the diffusion coefficient (0.104 $cm^2.s^{-1}$), supposing that the precursor gas is $H_2SO_4$
- r is the particle radius (cm)
- N is the particle number
- $\beta_{m,i}$ is the transitional correction factor, calculated as following

$$\beta m, i = \frac{Kn+1}{\frac{4}{3}Kn^2+1.7Kn+1} \quad (2)$$

- Kn is the Knudsen number, Kn = λ/r
- λ is the mean free path

The coagulation sink (CoagS) determines how fast fresh nucleated particles are lost through coagulation onto other particles.

The first step to calculate the coagulation sink is to calculate the coagulation coefficient. The coagulation coefficient between 2 particles of different diameters is calculated from Seinfeld and Pandis (2006):

$$K_{12} = \pi(R_{p1} + R_{p2})^2(c_1^2 + c_2^2)^{1/2} \quad (3)$$

Where

- $R_{p1}$: the ray of the first particle (m),
- $R_{p2}$: the ray of the second particle (m),
- $c_1$: the mean thermal velocity of the first particle ($m.s^{-1}$),
- $c_2$: the mean thermal velocity of the second particle ($m.s^{-1}$)

The mean thermal velocity is calculated as:

$$c_i = \sqrt{\frac{48 \times 1.38 \times 10^{-23} \times T}{\pi^2 \times \mu \times (\frac{D_i}{1000})^3 \times 10^{-18}}} \quad (4)$$

Where:

- T the temperature (K)
- μ the particle density ($kg.m^{-3}$)
- $D_i$ the diameter (nm)

This coefficient is calculated for each pair of diameters, so that we then obtain one coefficient per diameter as the sum of the coefficient between this diameter and all the others.

The coagulation sink is then obtained by:

$$CoagS = N_d \times K_d \quad (5)$$

where $N_d$ the number of particle for a diameter d, and $K_d$ the coagulation coefficient for a given diameter d. The coagulation sink is notably required for the calculation of the nucleation rate.

### b. Growth rate

The growth rate corresponds to the increase of the particles mean diameter (nm) per time (h). The method that we used to calculate it is similar to the one used in Dal Maso et al. (2005). The method was applied for each event independently.

To this end, the representation of the size distribution of the particles at a given time is needed. An example of the result is given Figure 10 a. On this figure, the x axis represents the diameter of the particles (in nm) measured in a log scale. The y axis gives the corresponding number of particles. We can see that the majority of the particles are situated in the nucleation mode, the first peak of the curve being for diameters around 15 nm. The move of this first mode to largest diameters over time traduces the particles growth. (Figure 10 b.)

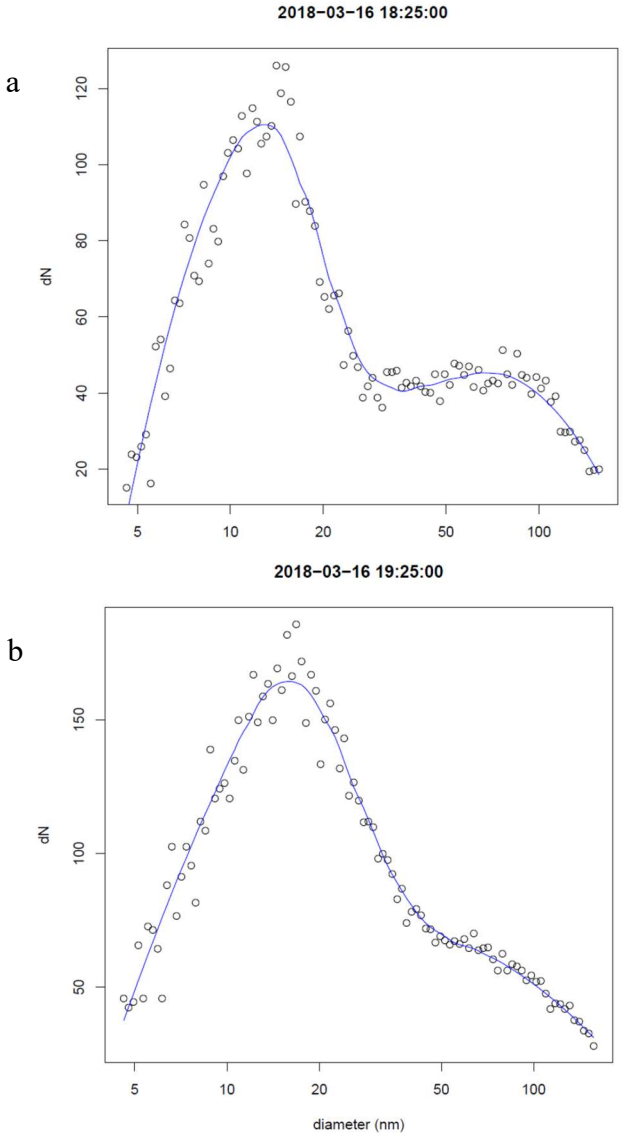


*Figure 10: a. Size distribution of particles on 16th March, 2018 at 18:25 (UT). b. Size distribution of particles on 16th March, 2018 at 19:25 (UT). Dots are measurements, the blue line represents the fitted curve obtained with the script developed using R.*

Therefore, I created a function on R to automatically fit the number distribution in order to calculate the diameter corresponding to the maximal concentration of the first mode. The obtained diameters at each time are also smoothed, and we finally obtain the diameter corresponding to first mode particles as a function of time over the whole event (see for example Figure 11).

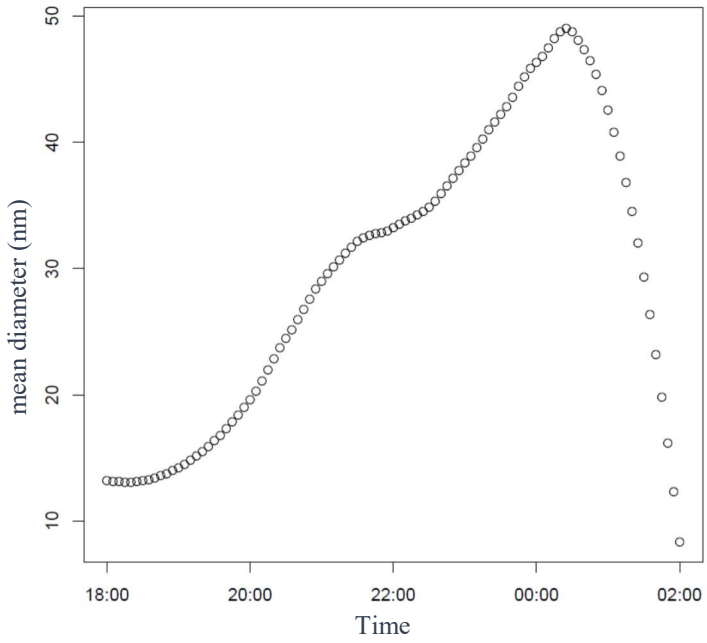


*Figure 11: Example of the evolution over time of the mean diameter of the first mode during a NPF event (observed on 2018-03-16)*

In Figure 11, we can see that the first mode diameter increases with time, representing the growth of the particles. To quantify this growth, the first mode diameter D was derived as a function of time (Kulmala et al., 2004):

$$GR = \frac{\Delta D}{\Delta t} \quad (6)$$

Where D is in nm and t in h, to obtain GR in $nm.h^{-1}$. This results in a GR for each time step (Figure 12).

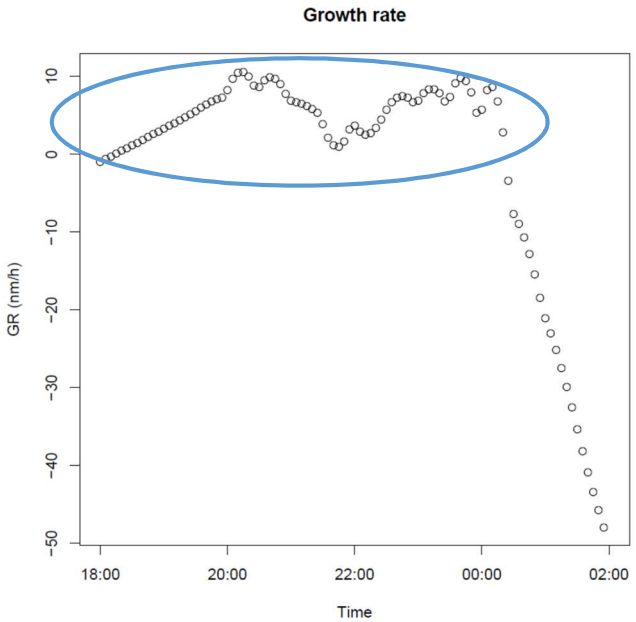


*Figure 12: Growth rates of 2018-03-16 event. The blue ellipse corresponds to the event period.*

We can see on Figure 12 that particles grew until midnight, then started to shrink. The wanted value is the mean growth rate over the event, which is thus calculated on the period before the GR sinks (blue ellipse on Figure 12). The negative values correspond to a decrease in particles concentration at the end of the event.

The whole R script developed to calculate growth rates can be found in Appendix 2.

### c. Nucleation rate

The nucleation rate represents how many nucleation clusters are formed by gas-particle conversion in a cubic centimetre of air. However, since critical clusters (size of 1-2 nm) are not measured in this study (because of the lower cut-off of the instrument, around 4 nm), the true nucleation rate cannot be obtained. Instead, the formation rate of a larger particle diameter was estimated, as commonly performed in other studies (Kulmala et al., 2001; Dal Maso et al., 2005; Hussein et al., 2008; Jaatinen et al., 2009).

It can be calculated as the formation of the smallest particles, here of 5 nm diameter, but it is often calculated as the formation of particles in the nucleation mode range, from 5 to 25 nm. The evolution of a particle population over time could be described as following (Kulmala et al., 2012):

$$\frac{\mathrm{dNdp}}{dt} = production - losses \quad (7)$$

With the production of particles being their formation, $J_{dp}$, and the losses corresponding to the sum of the losses by coagulation on bigger particles and by growth of the small particles, as they won't be in the size range anymore. $J_{dp}$ is calculated, for each time step, by (Dal Maso et al., 2005):

$$\frac{\mathrm{dNdp}}{dt} = J_{dp} - losses \rightarrow J_{dp} = \frac{\mathrm{dNdp}}{dt} + F_{coag} + F_{grow} \quad (8)$$

For a formation rate between 5- and 25nm-particles,

$$J_{5-25} = \frac{\Delta \mathrm{N}}{\Delta t} + F_{coag} + F_{growt} \quad (9)$$

Where

$$F_{coag} = N \times CoagS \quad (10)$$

$$F_{growt} = N \times GR_{5-25} \quad (11)$$

Considering only the particle size range between 5 and 25 nm, N is the total particle number at t, CoagS the coagulation sink at each time step and $GR_{5\text{-}25}$ the growth rate of particles at each time step.

A coagulation sink is calculated for each diameter (see equation 5), then the sum of all CoagS for each time step is calculated, obtaining the global CoagS per time.

From this, we obtain a table with $F_{coag}$, $F_{growth}$ and $\frac{\mathrm{dNdp}}{dt}$ for each time step, so that the sum of them provides $J_{5\text{-}25}$ for each time step.

An example of the obtained formation rate during a NPF event is presented on Figure 13.

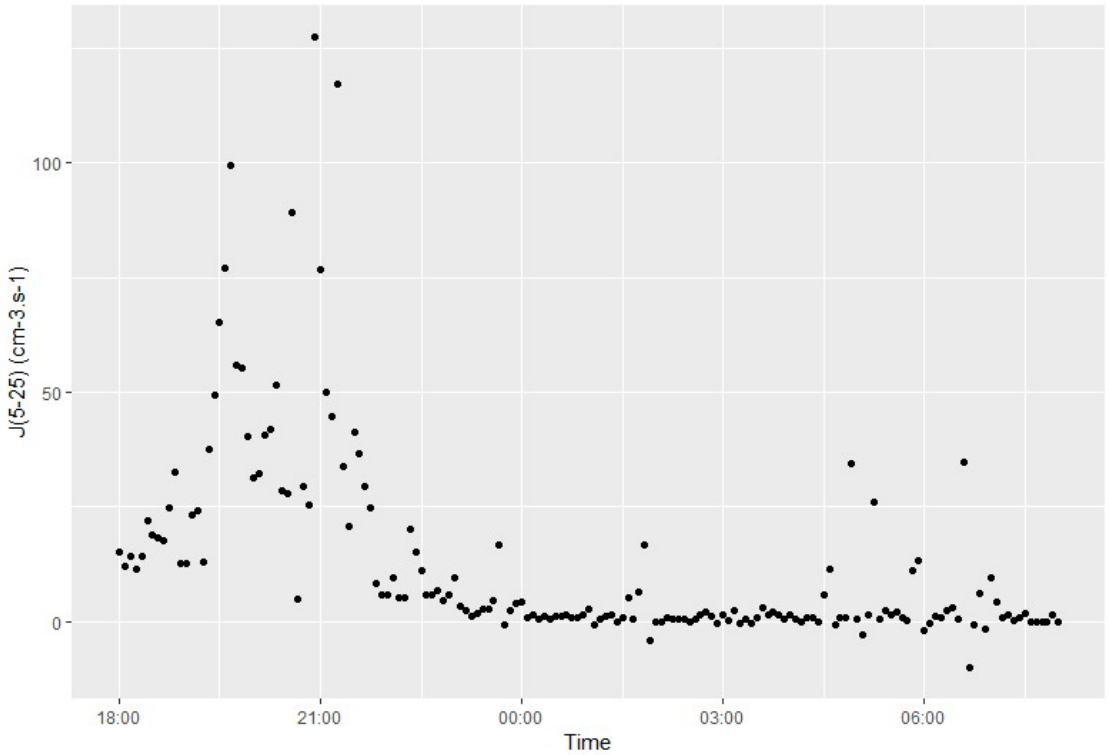


*Figure 13: Formation rate of 5-25 nm-particles for the nighttime event of 16th March, 2018*

From this example, I took the mean value during the nucleation phase (here from 18:05 to 22:40), i.e. when the nucleation rate increases, then sinks. This evaluation is of course subjective, but seems more relevant than taking the nucleation rate throughout the whole event, which makes little sense as soon as particles are larger than the nucleation mode.

# Chapter 5: Results & discussion

## I. Overview of the results

### 1) Observation of NPF events

Throughout the campaign, 15 NPF events were identified, which corresponds to 23% of the 65 days of the study. This is similar to a study conducted in winter in a suburban site in China, where NPF events represented 19% of the days over a year (Peng et al., 2017).

Among these 15 events, 8 occurred during the day and 7 during the night. The representations of all NPF events can be found in Appendix 3. An example of a daytime and a nighttime event is given in Figure 14. The first NPF event starts on April, 3rd around 5 PM (UT) and ends on April, 4th around 1 AM (UT). Several hours later a daytime event starts, around 9 AM (UT) until circa 9 PM. This configuration of 2 events happening successively is unique during the campaign, but has been seen in literature (Lee et al., 2008).

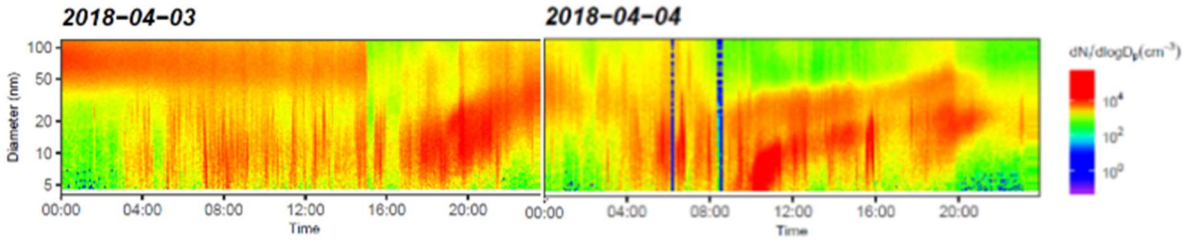


*Figure 14: Time variation of the particle number size distribution over two days of the campaign. The x axis is the time (in UT, whereas local time is UT+1, or UT+2 during daylight saving period), in y axis is the diameter (in nm, log scale) and the colour scale represents the concentration of particles (particle.cm$^{-3}$, log scale)*

The particle number concentration during the events is in the range $10^4$-$10^5$ particles.cm$^{-3}$. Even if it is not easy to see, we can observe that particle number concentration varies from one event to another.

An example of an unclear event is given in Figure 15. The typical shape of NPF is hardly discernible because of the presence of heavy particle loading during that moment.

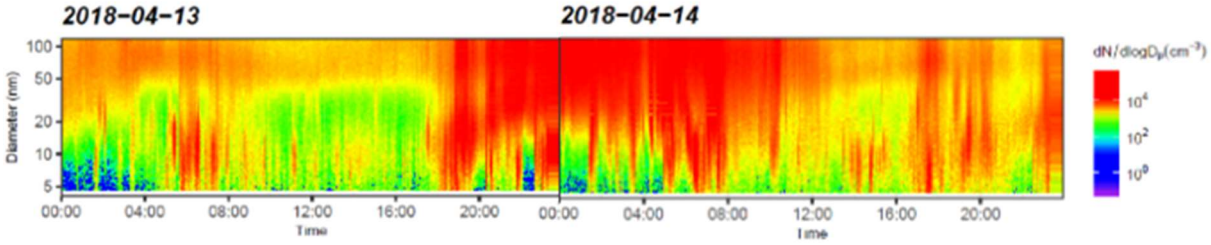


*Figure 15: Example of a nighttime unclear event*

Table 4 presents an overview of the main characteristics of these events. That is, first their start and end time (corresponding to the end of the growth phase); as it was not always easy to determine the exact end of growth, end times are given as more of an indication than a quantification parameter.

This table also gives mean ambient meteorological parameters during the event: air temperature (T°), relative humidity (RH) and wind speed (WS). Finally, mean physical variables are given: condensation sink (CS) during the nucleation phase, growth rate (GR) during the event and the formation rate of particles between 5 and 25 nm ($J_{5\text{-}25}$) during the nucleation phase.

*Table 4: Characteristics of the observed NPF events*

| NPF n° | category | Start date (UT) | End date (UT) | T° (°C) | RH (%) | WS ($m.s^{-1}$) | CS ($\times 10^3\ s^{-1}$) | GR ($nm.h^{-1}$) | $J_{5\text{-}25}$ ($cm^{-3}.s^{-1}$) |
|---|---|---|---|---|---|---|---|---|---|
| 1 | nighttime | 2018/03/13 17:00 | 2018/03/14 4:00 | 6.4 | 80.9 | 1.4 | 7.2 | 4.40 | 107.44 |
| 2 | nighttime | 2018/03/15 17:00 | 2018/03/16 1:00 | 9.2 | 81.7 | 3.6 | 5.0 | 4.44 | 9.60 |
| 3 | nighttime | 2018/03/16 18:00 | 2018/03/17 8:00 | 5.1 | 84.7 | 1.3 | 10.1 | 6.74 | 33.11 |
| 4 | nighttime | 2018/03/24 19:00 | 2018/03/25 7:00 | 7.6 | 70.8 | 0.7 | 33.6 | 4.05 | 63.29 |
| 5 | nighttime | 2018/04/03 17:00 | 2018/04/04 1:00 | 9.0 | 80.4 | 4.0 | 4.9 | 4.11 | 18.87 |
| 6 | daytime | 2018/04/04 9:00 | 2018/04/05 16:00 | 11.5 | 61.8 | 5.1 | 3.1 | 2.17 | 46.34 |
| 7 | nighttime | 2018/04/05 17:30 | 2018/04/06 2:00 | 6.8 | 61.1 | 2.4 | 14.6 | 4.63 | 168.98 |
| 8 | daytime | 2018/04/17 10:00 | 2018/04/18 3:00 | 16.1 | 52.7 | 2.0 | 8.4 | 3.75 | 62.95 |
| 9 | daytime | 2018/04/22 11:00 | 2018/04/22 17:00 | 24.2 | 37.4 | 4.0 | 9.8 | 3.36 | 22.88 |
| 10 | daytime | 2018/04/26 8:00 | 2018/04/27 8:00 | 10.4 | 58.9 | 2.4 | 4.4 | 2.05 | 53.32 |
| 11 | daytime | 2018/04/28 10:00 | 2018/04/28 16:00 | 13.4 | 52.3 | 3.0 | 5.2 | 2.72 | 37.82 |
| 12 | nighttime | 2018/04/28 19:00 | 2018/04/29 7:00 | 9.6 | 80.6 | 1.4 | 13.4 | 7.94 | 32.20 |
| 13 | daytime | 2018/05/07 11:00 | 2018/05/07 16:00 | 24.4 | 28.2 | 3.2 | 18.0 | 6.01 | 43.03 |
| 14 | daytime | 2018/05/09 9:00 | 2018/05/09 13:00 | 16.9 | 61.9 | 3.1 | 10.4 | 4.26 | 197.90 |
| 15 | daytime | 2018/05/10 9:00 | 2018/05/11 8:00 | 11.1 | 60.3 | 2.6 | 4.0 | 2.31 | 109.80 |

## 2) Meteorological parameters

The mean values of the meteorological parameters were calculated and are given in Table 5 with their corresponding standard deviation.

*Table 5: Mean values of temperature, relative humidity and wind speed for nighttime and daytime events*

| | daytime | nighttime |
|---|---|---|
| T° (°C) | 16.0 ± 5.6 | 7.7 ± 1.7 |
| RH (%) | 51.7 ± 12.5 | 77.2 ± 8.3 |
| WS ($m.s^{-1}$) | 3.2 ± 1.0 | 2.1 ± 1.2 |

The mean temperature and the mean wind speed were lower for nighttime events, whereas the relative humidity was higher. In fact, in general nights are colder, steadier, and more humid than days. This suggests that the conditions for NPF events are different between daytime and nighttime.

## 3) Nucleation and growth properties

The physical variables enable a quantitative comparison between the events. We can observe an important variability of the nucleation rate, with particularly high values for events 7 and 14 regarding the other events (Table 3). This variability of the nucleation rate is in agreement with the observed NPF events. For example, Figure 16 shows two NPF events (event 5 and event 7) that have completely different nucleation rates.

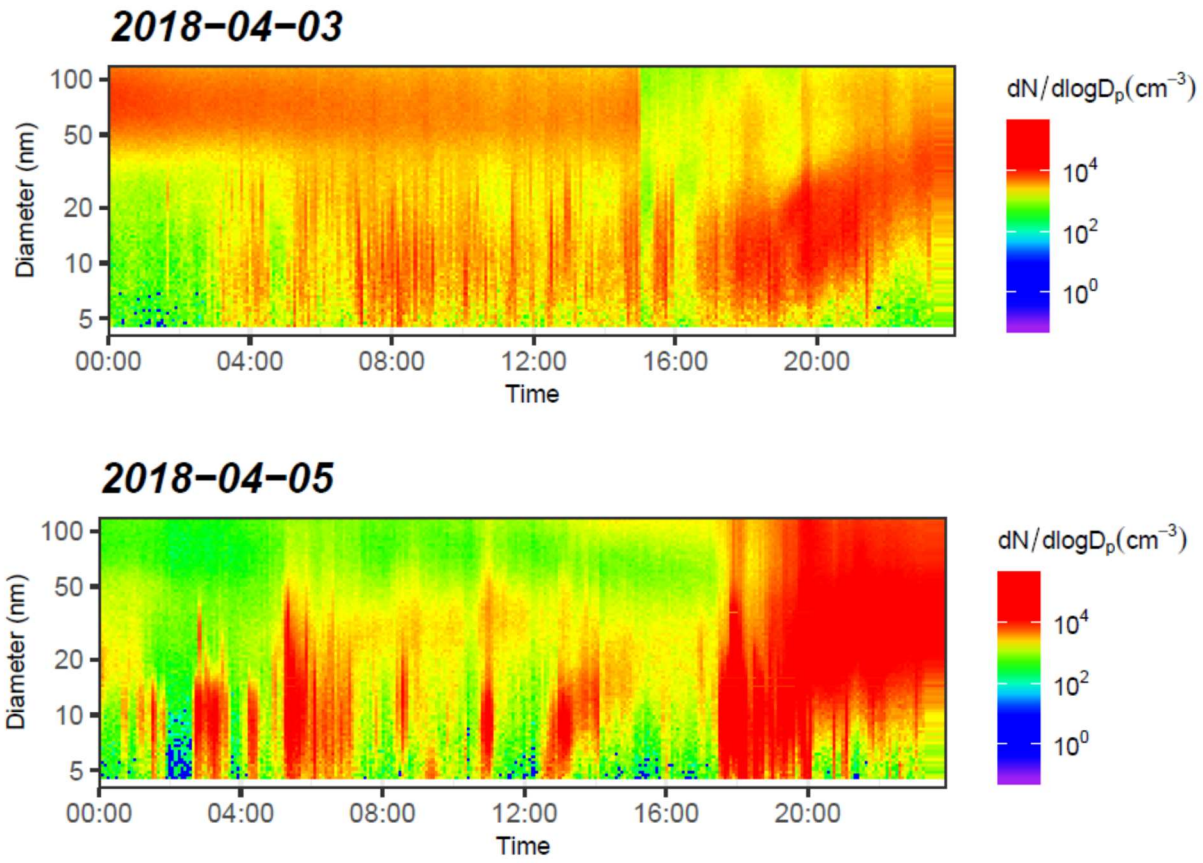


*Figure 16: Number size distribution during 3rd and 5th April 2018 for quantitative comparison*

The first event (event 5) on Figure 15 has a low nucleation rate (18.87 $cm^{-3}.s^{-1}$), whereas the second one (event 7) has a much higher nucleation rate value (168.98 $cm^{-3}.s^{-1}$). This contrasts with their close growth rates (4.11 $nm.h^{-1}$ for event 5, 4.63 for event 7). There seems to be no correlation between nucleation rate and growth rate here. This suggests that the processes, conditions and involved precursors might be different for nucleation and condensation.

From the values of Table 4, I calculated the mean condensation sink, growth rate and nucleation rate for both daytime and nighttime events, as well as their standard deviation (Table 6). The growth rates showed a clear difference between nighttime and daytime events, whereas the nucleation rates were more similar. The mean condensation sink and growth rate were higher for nighttime events, but the nucleation rate was higher for the daytime events. In fact, daytime events were in general more intense than the nighttime ones. The growth rate varied from an event to another from around 2 to 8 $nm.h^{-1}$ and the nucleation rate varied from 10 to 200 $cm^{-3}.s^{-1}$.

It is thus important to consider that daytime and nighttime events differ significantly and must be treated separately.

*Table 6: Mean values of CS, GR and $J_{5-25}$ for nighttime and daytime events*

| | nighttime | daytime |
|---|---|---|
| CS | $13 \pm 10.10^{-3}$ $s^{-1}$ | $7.9 \pm 4.9.10^{-3}$ $s^{-1}$ |
| GR | $5.32 \pm 1.63$ $nm.h^{-1}$ | $3.33 \pm 1.34$ $nm.h^{-1}$ |
| $J_{5-25}$ | $61.93 \pm 57.50$ $cm^{-3}.s^{-1}$ | $71.76 \pm 57.06$ $cm^{-3}.s^{-1}$ |

The comparison for nocturnal events was not easy to do, as the few studies that report some observations were either done in different environments (with purely biogenic emissions for example), or these variables were not calculated.

For a comparison of the daytime events with previous studies, it is also important to note that the measurements were done in a suburban environment. Only few studies were done in such environment, so we also compared with measurements in urban environments.

Jaatinen et al. (2009) studied NPF events in a rural site in a polluted area in Germany. Their observed formation rate was about $J_{3-25} = 4.6$ $cm^{-3}.s^{-1}$. Hussein et al. (2008), at an urban site in Finland, obtained a $J_{3-25}$ of 2.4 $cm^{-3}.s^{-1}$. Wu et al. (2007) conducted a study in the outskirts of Beijing (China). They observed a mean formation rate of $J_{3-25} = 16.2$ $cm^{-3}.s^{-1}$ for "polluted" NPF events (with air masses coming from the city) and of 22.3 $cm^{-3}.s^{-1}$ for "clean" events (Figure 17 a.) A higher nucleation rate for clean events can be due to a lower CS at the start and a lower particles number concentration.

The nucleation rates are thus smaller than the ones that we obtained. The growth rates are of the same order of magnitude in these studies, and similar to the ones observed in our study (Wu et al., 2007; Hussein et al., 2008; Jaatinen et al., 2009). Jaatinen et al. (2009) reported a growth rate around 6.2 $nm.h^{-1}$, Hussein et al. (2008) around 3.8 $nm.h^{-1}$, and Wu et al. (2007) a growth rate of 1.8 $nm.h^{-1}$ for "clean" events and of 4.4 $nm.h^{-1}$ for "polluted" event (Figure 17 b.), suggesting a correlation between pollutant concentration and particle growth.

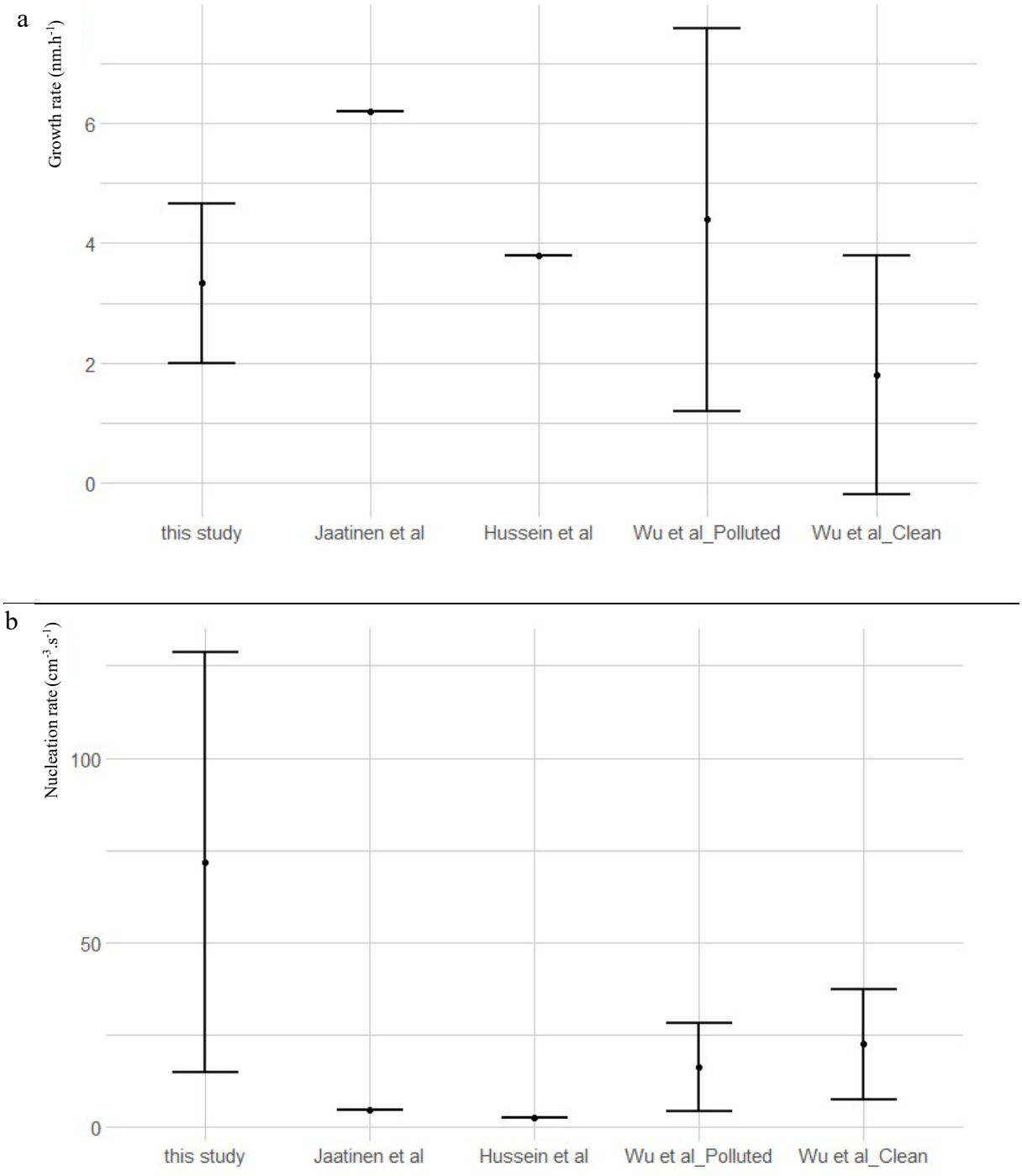


*Figure 17: Comparison of the mean GR (a.) and J (b.) and their corresponding standard deviation*

# II. Conditions favouring NPF events

Daytime and nighttime events were to be analysed independently, so we separated all days and all nights into the categories of "NPF event", "unclear", or "non-event", according to the criteria presented in Chapter 4, Table 6.

The obtained datasets for each category of days and nights enabled to create diurnal and nocturnal profiles of all parameters and to analyse them in order to highlight conditions favouring the events. All profiles can be found in the Appendixes 3 and 4, while only the most relevant ones will be shown and explained in this section.

## 1) Daytime

The main process involved in the formation of new particles is the oxidation of organic compounds, producing heavier species, that will become semi-volatile and thus will easily condense. Species like ozone ($O_3$) and hydroxyl radical (OH), whose production is photo-induced, might oxidize gaseous compounds.

The diurnal profiles of Photosynthetic Photon Flux Density (PPFD), that quantifies solar radiation, and ozone are shown on Figure 18.

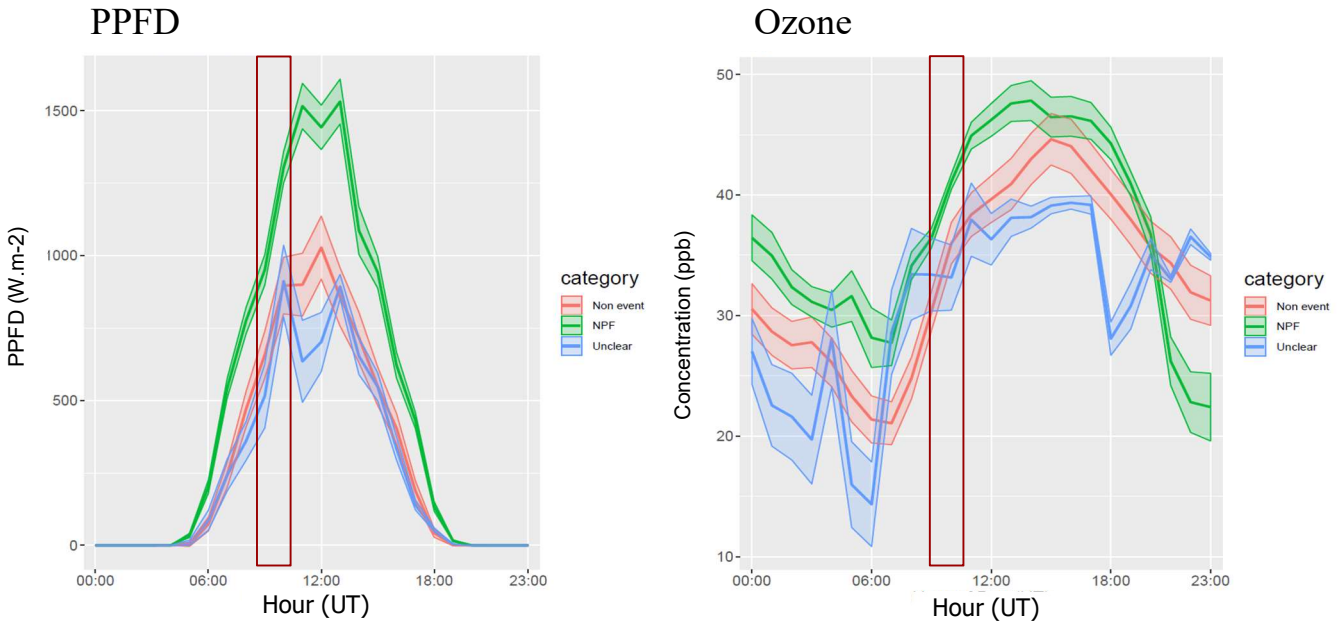


*Figure 18: Diurnal profiles of Photosynthetic Photon Flux Density and ozone concentration. The green line represents NPF days, the blue line represents unclear days and the red line represents non-event days. The red rectangle represents the start of the event.*

The median maximum PPFD is situated for NPF events around 1500 $W.m^{-2}$, while for unclear and non-event days, it is situated around 1000 $W.m^{-2}$ or less. The maximum concentration of $O_3$ during NPF event days is around 47 ppb, while it is around 40-45 ppb for unclear and non-event days.

Thus, the observed tendency is a higher solar radiation and a higher level of $O_3$ for the overall NPF event during the day. In order to best study the nucleation phase, it is necessary to look at the start time of the event, around 9 AM-11 PM. There, we can also observe a higher level of solar radiation and of ozone concentration as well, which both might favour a nucleation process. Both diurnal profiles suggest that photochemistry is involved in the daytime NPF at the FR-Gri site.

In several studies (Kulmala et al., 2004; Paasonen et al., 2010; Sipilä et al., 2010; Yue et al., 2010), sulphuric acid was found to be a major precursor of secondary particles. Indeed, it plays a particular role in the nucleation step and is formed from sulphur dioxide photooxidation. Unfortunately, $H_2SO_4$ was not directly measured during the campaign but can be estimated using the concentration of $SO_2$ and the PPFD.

$SO_2$ was also not measured on the site, but since it is quite homogeneous within the region around Paris (Bressi et al., 2013), the values were taken from regional monitoring network of air quality (Airparif). The proxy for $H_2SO_4$ was calculated as recommended by Mikkonen et al. (2011):

$$[H_2SO_4] = 8.21.10^{-3} \times k \times PPFD \times [SO_2]^{0.62} \times (CS \times RH)^{-0.13} \quad (9)$$

Where:
- k the reaction rate of $SO_2$ to $H_2SO_4$,
- PPFD the solar radiation,
- CS the condensation sink,
- RH the relative humidity

Diurnal variation of the obtained $H_2SO_4$ proxy is presented in Figure 19 and its concentration is also higher during NPF days than unclear and non-event days, which is rather logical given the strong dependency on PPFD (Equation 9). This result indirectly suggests that, as already observed in other sites, $H_2SO_4$ is one of the key parameters driving NPF during the day.

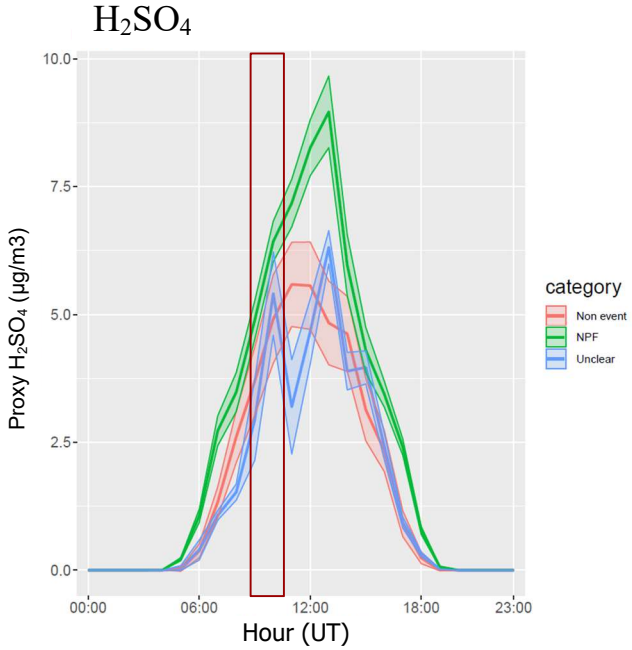


*Figure 19: Diurnal profile of proxy $H_2SO_4$*

Another striking feature of my results is the temporal variability of the starting time (Table 4). To better understand this discrepancy, a comparison event by event was made, as well as a comparison with a couple of non-event days.

The main contribution factors, i.e. ozone, PPFD, proxy $H_2SO_4$ and the condensation sink, were represented as time series for all daytime events. Figure 20 gives two significant examples that will be detailed. Other examples can be found in Appendix 5.

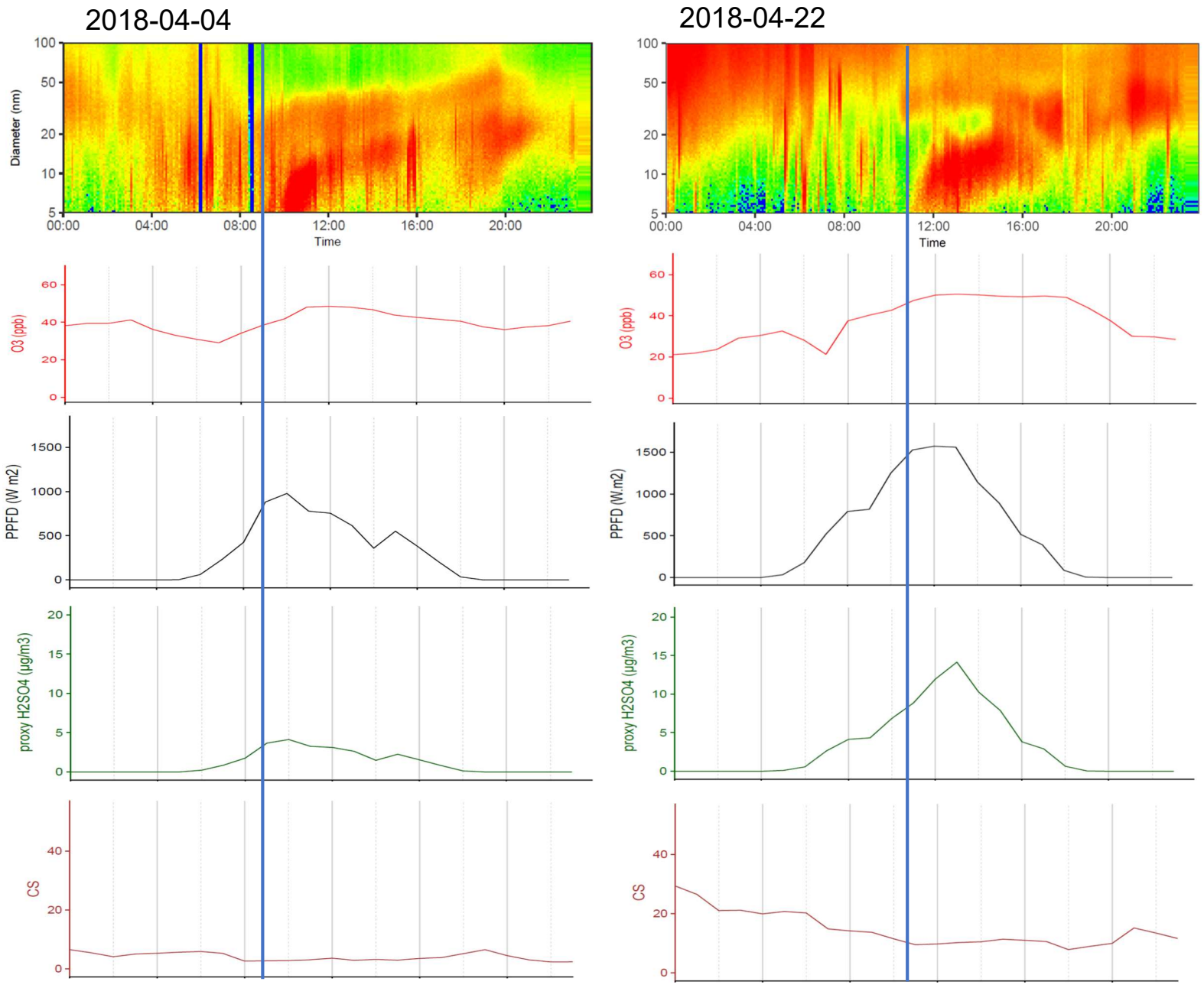


*Figure 20: Time series of 2 daytime events, April, 4th and April 22nd, as well as the time series of some parameters on these days. All x axes are the same as the above one. The vertical blue line represents the start of the event.*

Different trends can be observed for these time series. On the left is a daytime event that start quite early, around 9 AM (UT); and on the right a daytime event that start later, around 11 AM (UT). Their conditions are different: on April 4th, the levels of $O_3$, PPFD and sulphuric acid were lower than on April 22nd. Moreover, on April 4th, the condensation sink was very low, whereas it was not really the case for April 22nd.

The explanation may be that some events (like April 4th) don't need too much solar radiation and sulphuric acid concentration to occur – just enough to condense, which is possible with a CS very low at the start of the event, because the competition between nucleation and condensation on pre-existing particles can be in favour of nucleation. A minimum amount of sulphuric acid can be enough to produce particulate nuclei.

On the other hand, some events (like April 22nd) will only happen if the solar radiation, ozone and sulphuric acid concentrations are very high, allowing the formation of new particles despite a higher CS. Nucleation can only happen if the concentration of gaseous molecules is high enough. If start time variability has been observed before (Held et al., 2004; Jung et al., 2013), to my knowledge no such tendency has been reported in the literature.

To better understand this difference in conditions and to verify its application on all daytime events, Table 7 summarizes some of the characteristics of all daytime events. The characteristics are the numeration of the event, its start time, the time corresponding to the end of nucleation, then of growth. CS, total PM concentration, and $H_2SO_4$ were averaged on the nucleation phase, PPFD was averaged +/- 30 min of start time, $O_3$ was averaged on the whole event and the growth rate was averaged on the growth phase.

Thanks to all this, it was possible to separate them into 2 types: the "early" type, and the "late" type.

*Table 7: Some characteristics of daytime events*

| NPF N° | event start (UT) | end nucleation (UT) | end growth (UT) | CS ($\times 10^2$ s$^{-1}$) | PPFD (W/m$^2$) | $O_3$ (ppb) | PM tot (µg/m$^3$) | $H_2SO_4$ (µg/m$^3$) | GR (nm.h$^{-1}$) | Type |
|---|---|---|---|---|---|---|---|---|---|---|
| 6 | 2018/04/04 09:00 | 2018/04/04 11:45 | 2018/04/04 16:00 | 3.1 | 790.67 | 45.11 | 1.29 | 2.76 | 2.17 | early |
| 8 | 2018/04/17 10:00 | 2018/04/17 12:15 | 2018/04/18 3:00 | 8.4 | 1270.30 | 34.08 | 1.66 | 5.65 | 3.75 | late |
| 9 | 2018/04/22 11:00 | 2018/04/22 16:00 | 2018/04/22 17:00 | 9.8 | 1500.40 | 49.49 | 3.96 | 11.65 | 3.36 | late |
| 10 | 2018/04/26 08:00 | 2018/04/26 12:50 | 2018/04/27 00:00 | 4.4 | 749.00 | 35.28 | 1.49 | 5.45 | 2.05 | early |
| 11 | 2018/04/28 10:00 | 2018/04/28 13:55 | 2018/04/28 16:00 | 5.2 | 822.79 | 42.26 | / | 6.33 | 2.72 | early |
| 13 | 2018/05/07 11:00 | 2018/05/07 16:00 | 2018/05/07 16:00 | 18.0 | 1983.68 | 60.59 | 8.04 | 8.43 | 6.01 | late |
| 14 | 2018/05/09 09:00 | 2018/05/09 10:45 | 2018/05/09 13:00 | 10.4 | 1239.93 | 34.91 | / | 4.90 | 4.26 | late |
| 15 | 2018/05/10 09:00 | 2018/05/10 18:00 | 2018/05/11 08:00 | 4.0 | 669.18 | / | / | 6.11 | 2.31 | early |

The results are in agreement with what was discussed using Figure 20. In fact, the events that start early (shortly after sunrise) have lower CS, PPFD, concentration of particles, and

concentration of sulphuric acid than events that start later. The start time is actually not the only influencing factor, but rather the totality of the above mentioned ones.

The growth rate seems to be lower for "early" events than for "late" events. This could be explained by the higher solar radiation for "late" events at the start time, but also throughout the event. Thus, more photochemical activity takes place and more gaseous precursors can condense to the particle phase.

The study of the same parameters during non-event days, showed that the CS and PM concentrations were too high and the PPFD was too low to enable nucleation and/or growth processes.

## 2) Nighttime

The nighttime events were more difficult to understand, as they are in general less observed. There is no nucleation scheme as for daytime nucleation, where the role of $H_2SO_4$ and photochemistry have been evidenced (Kulmala et al., 2004).

Figure 21 a. shows the nocturnal profile of ammonia ($NH_3$). $NH_3$ concentration is higher for the nights in which there is a NPF event (green line on Figure 21).

Thus, the presence of high concentrations of ammonia may favour the occurrence of NPF events. In France, agriculture is responsible for about 97% of the emissions of $NH_3$ (ADEME, 2012). This may link NPF events at the FR-Gri site to an agricultural source.

Nucleation processes involving ammonia are described in the literature (Kulmala et al., 2000). $NH_3$ enhances indirectly NPF with a catalysis role during the oxidation stage, and directly with a neutralizing role in the aggregation stage (Jiang and Xia, 2017). By increasing pH, $NH_3$ might promote oxidation of $NO_2$ to $NO_3^-$.

Figure 21 b. represents the nocturnal profile of nitrogen dioxide. Its concentration is higher on NPF days than on non-event days. $NO_2$ might also favour the occurrence of NPF, especially with its ability to form $NO_3^-$, a precursor of the inorganic fraction of new particles.

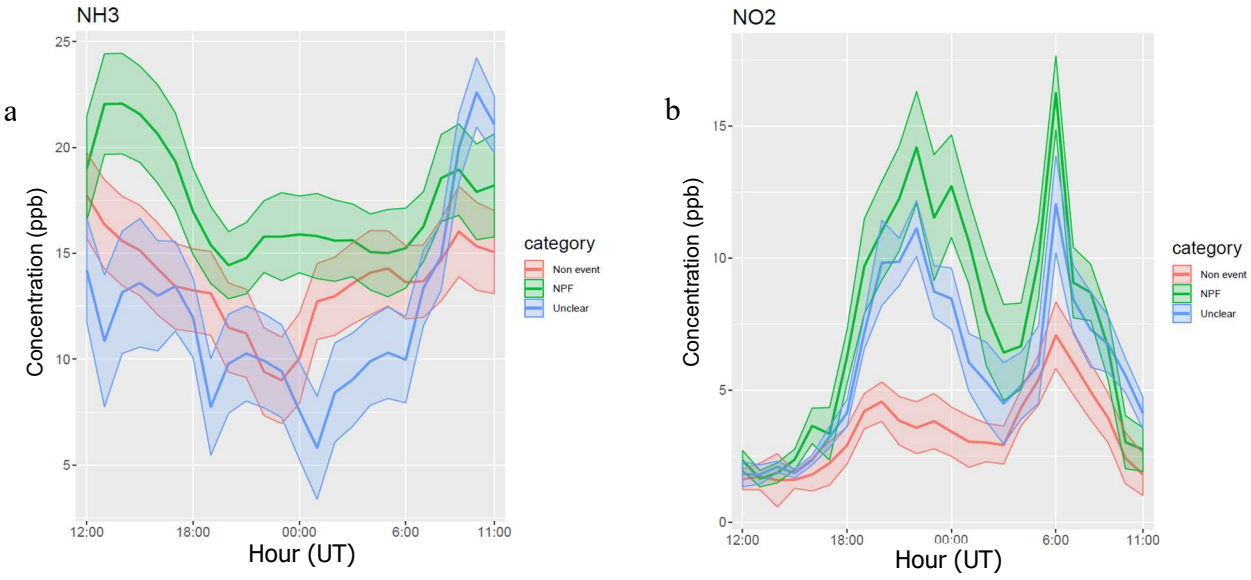


*Figure 21: a. Nocturnal profile of ammonia ($NH_3$) b. Nocturnal profile of nitrogen oxide ($NO_2$)*

$NO_2$ is also involved in the production of nitrate radical ($NO_3$). During daytime, this radical is photolysed. At night, while its production through $NO_2$ and $O_3$ is still possible, even if $O_3$ levels are lower, $NO_3$ is not suppressed and can react with gaseous species to form secondary particles (Chen et al., 2019).

$NO_2$, as well as the fraction of black carbon from fossil fuels ($BC_{ff}$), is a tracer for emissions due to traffic (Sandradewi et al., 2008). The nocturnal profile of $BC_{ff}$ is given Figure 22 a. For NPF events, we can see a peak around 8-9 PM on both $NO_2$ and $BC_{ff}$ profiles, showing that they are probably linked.

If nucleation occurs sooner (around 7 PM) and might not be affected by these compounds, the growth phase however could be favoured by their increase.

Figure 22 b. represents the nocturnal profile of black carbon from wood burning activities ($BC_{wb}$). This profile also shows a peak on NPF events during the night (around 10-11 PM). With the two-hours offset with local time, it is hard to assign these peaks to their usual sources.

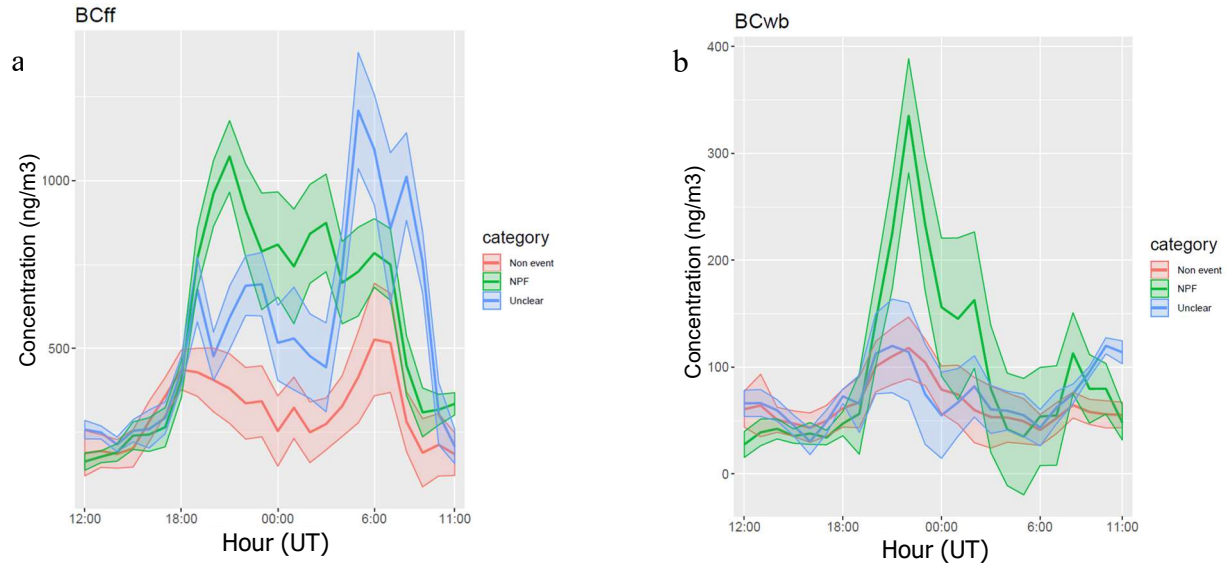


*Figure 22: a .Nocturnal profiles of black carbon from fossil fuels (BCff). b. Nocturnal profile of black carbon from wood burning (BCwb)*

By linking these results to the Inverse U star (where U* is the friction velocity in $m.s^{-1}$, expressing the turbulence intensity), a parameter that represents the stratification of the air, we saw the same peak around 9-10 PM (Figure 23).

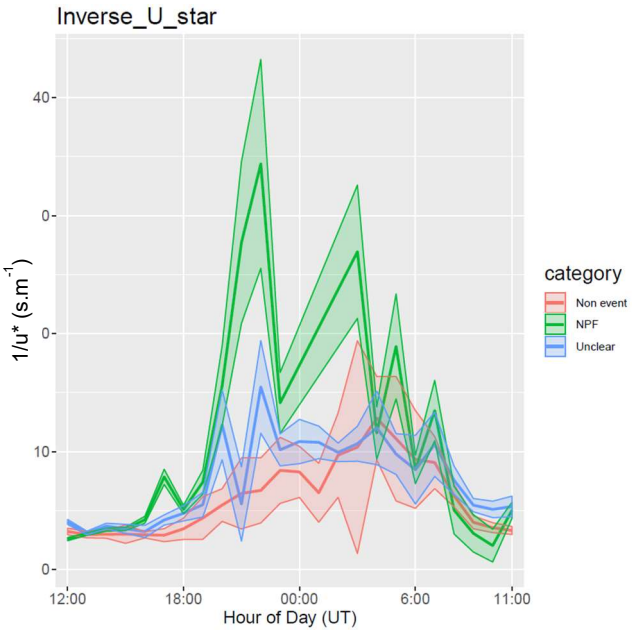


*Figure 23: Nocturnal profile of inverse u star (1/u*), representing the stratification of the air*

To comprehend how this might affect the atmospheric chemistry occurring at night, it is important to understand the atmospheric dynamic of the surface layer.

Figure 24 gives a schematic view of the troposphere and the boundary layer, the layer closest to the ground and where chemical reactions between emitted compounds might occur.

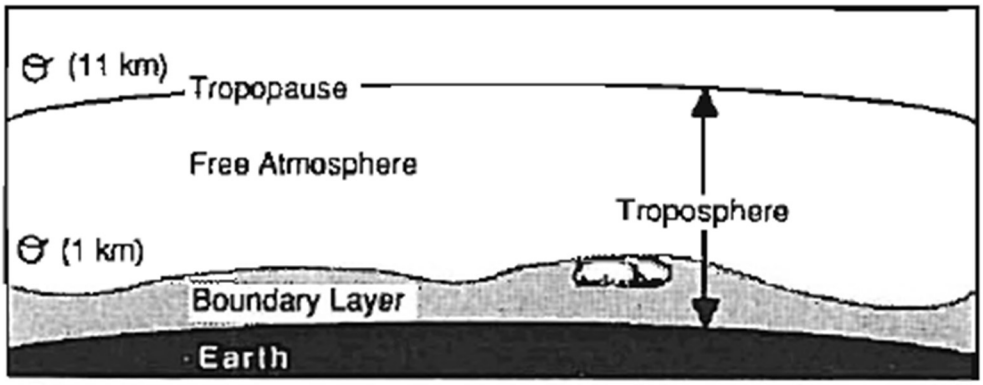


*Figure 24: First layer above the Earth: the troposphere, that is divided into the boundary layer and the free atmosphere (Stull, 1988)*

The boundary layer, in which we performed our measurements, is especially important for the reactions and transformations that take place in the troposphere, because it is located directly on the Earth's surface. Figure 25 shows the diurnal variation of the boundary layer (BL).

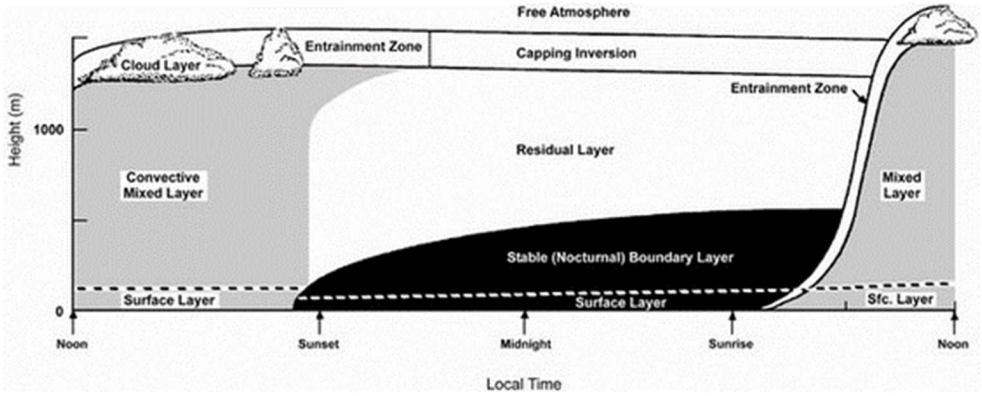


*Figure 25: The diurnal variation of the tropospheric layers (Stull, 1988)*

The three major components of the troposphere are the convective BL, the residual layer and the nocturnal BL, which is formed after sunset. The mixed layer, or boundary layer, is the atmospheric layer in which constituents or pollutants present within this layer, are dispersed by turbulence during the day. At night, the mixed layer height is often located near the ground, with accumulates pollutants in the shallow mixed layer (Stull, 1988; Wagner and Schäfer, 2017).

The increase of 1/u* that was observed during nighttime NPF events shows that the nocturnal BL is more stable on these nights than during nights of non-event. Pollutants will stay together instead of being pushed away by the wind, which might favour reactions of oxidation and have an impact on NPF events.

The involvement of nighttime atmospheric chemistry implies that the events might occur on a regional scale. To discriminate between a local implication of agricultural activities and a regional process, the observations on the FR-Gri site were compared to a regional background measurement station (SIRTA).

## III. Comparison with a background site

The SIRTA observatory, located 27 km SE of Grignon, is also equipped with many instruments allowing the characterization of the gas and particle phases of the background area of suburban Paris, and the Île de France region (Figure 26).

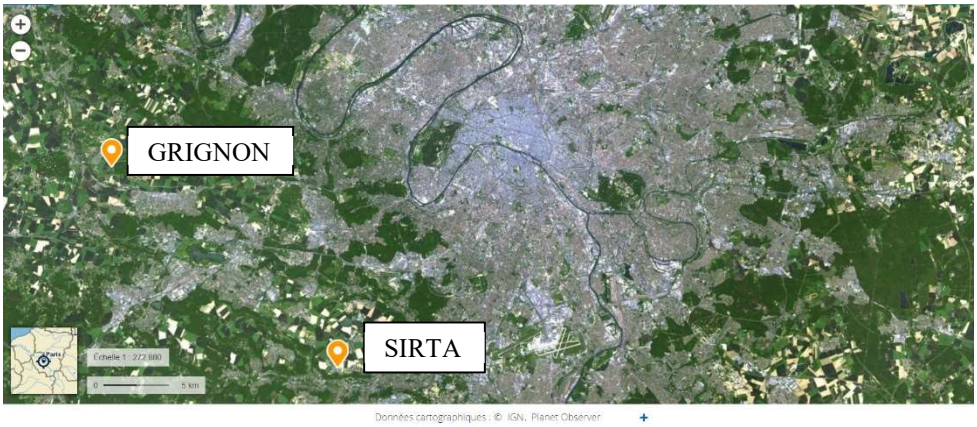


*Figure 26: Location of Grignon and the SIRTA station (IGN, 2019)*

During the same period than the campaign, particle number size distribution was also measured at SIRTA. The same analysis of this dataset was carried out, in order to identify NPF events.

Figures 27 and 28 give examples of this observation for a daytime and a nighttime event, respectively. It is important to note that the instruments used were different, and the colour scale of the graphs is different.

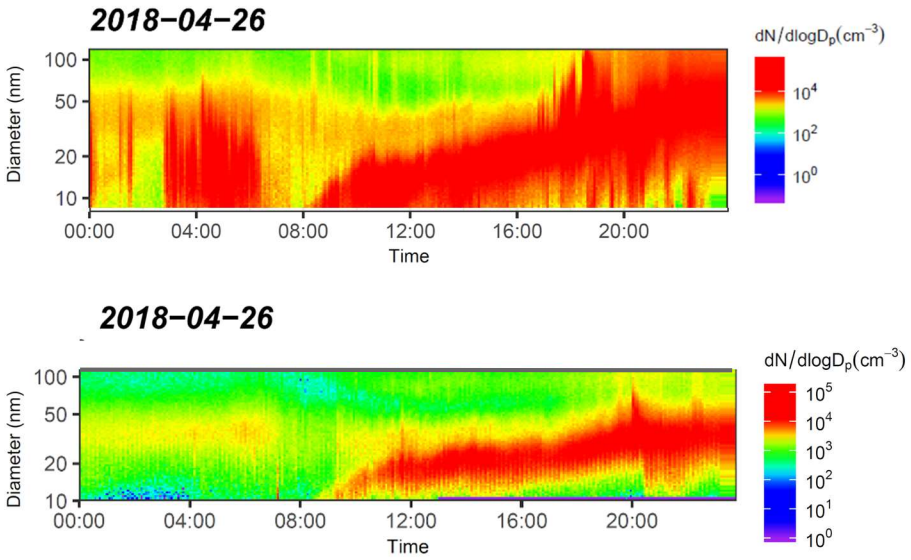


*Figure 27: Daytime event on April 26th, occurring at both Grignon (above) and the SIRTA (below)*

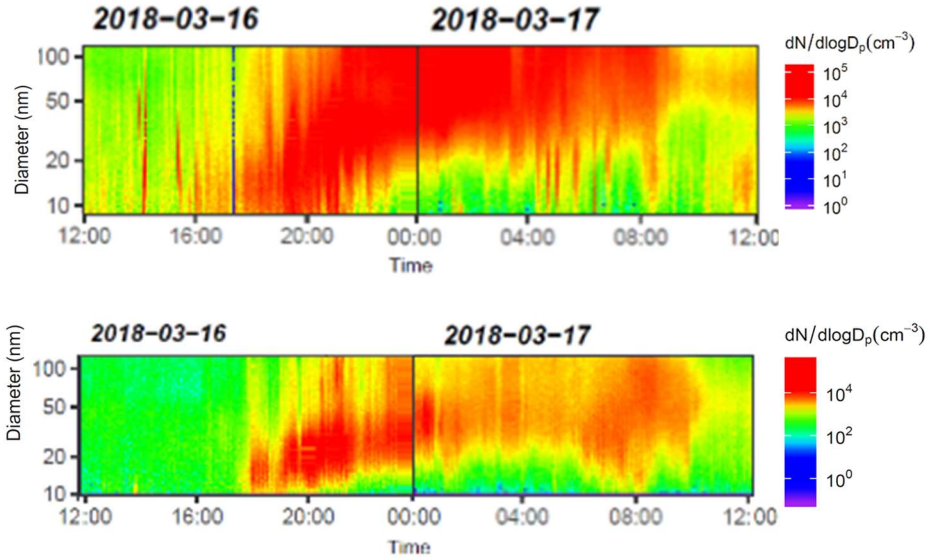


*Figure 28: Nighttime event on March 16th, that occurred both at Grignon (above) and at the SIRTA station (below)*

Because of this difference of instrument and scale, it is not possible to compare the measurements on both sites quantitatively. However, we can still observe, from Figures 27 and 28, that the events occurred on both sites almost simultaneously. It was the case for all events, except for the 8th event in Grignon. The small temporal difference could be due to transport, or concentration, as the concentration scales are different.

This observation suggests that the events are regional, and not local.

Daytime regional events have already been observed (Shen et al., 2011), but this result is more surprising for nighttime events. In fact, daytime NPF being driven by solar radiation, $SO_2$ concentration and $O_3$, which are quite homogeneous in the suburbs of Paris, it is logical that these events are regional.

For the nighttime events, as mentioned before, the atmospheric dynamic plays a role, and is also the same over the region. Moreover, if ammonia, and potentially agricultural activities, has an impact on the occurrence of nighttime events, it would be on a regional scale.

# Conclusion

The objective of my internship consisted in the characterization of new particle formation events in an agricultural-suburban environment. To do so, this work focused on the analysis of an existing dataset from an in-situ measurement campaign which took place at Grignon (West of Paris) in 2018. The number size distribution of particles was used to highlight NPF events, and collocated physical and chemical measurements helped to investigate the conditions favouring the occurrence of these events.

During the 65 days of the campaign, 8 daytime and 7 nighttime events were identified. Nighttime events are rare in the literature, but here they represented half of our observations. Calculated nucleation rates were on average higher for daytime events, while the mean growth rate was higher for the nighttime ones. For daytime events, nucleation rates were higher than what is generally reported in literature, whereas growth rates were in the same order of magnitude regarding other urban and suburban sites.

Higher solar radiation, ozone and estimated sulphuric acid levels were found for daytime events compared to non-event days, suggesting that nucleation is induced by the gas-particle conversion of sulphuric acid, and that growth may be due to the condensation of oxidized compounds on newly formed particles, two processes well described in the literature. An interesting feature lies in the variability of the start time of these events.

They were separated into two categories, “early” and “late” events, whose conditions differed. Early events occurred for low number of pre-existing particles, and started as soon as there was enough solar radiation, ozone and sulphuric acid for nucleation. On the other hand, late events, for which the number concentration of pre-existing particles was higher, could only occur if the solar radiation, ozone and sulphuric acid levels were high enough to favour nucleation over condensation on pre-existing particles.

As for nighttime events, higher concentrations of ammonia, known to catalyse nucleation, suggest a link with agricultural activities. Higher concentrations of nitrogen dioxide and black carbon during the night, as well as meteorological parameters suggesting steadier conditions, indicates that these variabilities might be more related to the decrease of the boundary layer than direct emission, which could enhance nucleation. Moreover, $NO_2$ can form $NO_3$ that can oxidize volatile compounds, enabling their condensation onto new particles.

It was the first time that NPF events were observed in an agricultural environment, both daytime and nighttime. A comparison with a background site showed that these events occurred on a regional scale.

A further analysis of precursors gaseous compounds can be considered, in order to better characterize NPF event in an agricultural site.

# References

ADEME, 2012. Agir pour limiter l'impact de l'agriculture 19.

Brégonzio, L., 2013. Formation d'aérosols organiques secondaires au cours de la photooxydation multiphasique de l'isoprène 261.

Bressi, M., Sciare, J., Ghersi, V., Bonnaire, N., Nicolas, J.B., Petit, J.-E., Moukhtar, S., Rosso, A., Mihalopoulos, N., Féron, A., 2013. A one-year comprehensive chemical characterisation of fine aerosol (PM2.5) at urban, suburban and rural background sites in the region of Paris (France). Atmospheric Chem. Phys. 13, 7825–7844.

Chen, X., Wang, Haichao, Liu, Y., Su, R., Wang, Hongli, Lou, S., Lu, K., 2019. Spatial characteristics of the nighttime oxidation capacity in the Yangtze River Delta, China. Atmos. Environ. 208, 150–157.

Curtius, J., 2009. Nucleation of atmospheric particles. Eur. Phys. J. Conf. 1, 199–209.

Dal Maso, M., Kulmala, M., Riipinen, I., Wagner, R., Hussein, T., Aalto, P.P., Lehtinen, K.E.J., 2005. Formation and growth of fresh atmospheric aerosols: eight years of aerosol size distribution data from SMEAR II, Hyytiälä, Finland 10, 15.

Dameto de España, C., Wonaschütz, A., Steiner, G., Rosati, B., Demattio, A., Schuh, H., Hitzenberger, R., 2017. Long-term quantitative field study of New Particle Formation (NPF) events as a source of Cloud Condensation Nuclei (CCN) in the urban background of Vienna. Atmos. Environ. 164, 289–298.

Gao, S., Lathem, T., Nyadong, L., 2019. Nighttime secondary organic aerosol formation from unburned fuel vapors. Atmos. Environ. 204, 125–134.

Gooch, J.W., 2011. Vapor Pressure, in: Gooch, J.W. (Ed.), Encyclopedic Dictionary of Polymers. Springer New York, New York, NY, pp. 789–789.

Gros, V., Baisnée, D., Bedos, C., Bonnaire, N., Bsaibes, S., Buysse, P., Decuq, C., Kammer, J., Lafouge, F., Sarda-Estève, R., Truong, F., 2019. Rapport intermédiaire AgriMultiPol 35.

Held, A., Nowak, A., Birmili, W., Wiedensohler, A., Forkel, R., Klemm, O., 2004. Observations of particle formation and growth in a mountainous forest region in central Europe. J. Geophys. Res. Atmospheres 109.

Hussein, T., Martikainen, J., Junninen, H., Sogacheva, L., Wagner, R., Maso, M.D., Riipinen, I., Aalto, P.P., Kulmala, M., 2008. Observation of regional new particle formation in the urban atmosphere. Tellus B Chem. Phys. Meteorol. 60, 509–521.

Jaatinen, A., Hamed, A., Joutsensaari, J., Mikkonen, S., Birmili, W., Wehner, B., Spindler, G., Wiedensohler, A., Decesari, S., Mircea, M., Facchini, M.C., Junninen, H., Kulmala, M., Lehtinen, K.E.J., Laaksonen, A., 2009. A comparison of new particle formation events in the boundary layer at three different sites in Europe. Boreal Environ. Res. 14, 18.

Jiang, B., Xia, D., 2017. Role identification of NH3 in atmospheric secondary new particle formation in haze occurrence of China. Atmos. Environ. 163, 107–117.

Jung, J., Miyazaki, Y., Kawamura, K., 2013. Different characteristics of new particle formation between urban and deciduous forest sites in Northern Japan during the summers of 2010–201. Atmos Chem Phys 19.

Kammer, J., Perraudin, E., Flaud, P.-M., Lamaud, E., Bonnefond, J.M., Villenave, E., 2018. Observation of nighttime new particle formation over the French Landes forest. Sci. Total Environ. 621, 1084–1092.

Kerminen, V.-M., Chen, X., Vakkari, V., Petäjä, T., Kulmala, M., Bianchi, F., 2018. Atmospheric new particle formation and growth: review of field observations. Environ. Res. Lett. 13, 103003.

Kroll, J.H., Seinfeld, J.H., 2008. Chemistry of secondary organic aerosol: Formation and evolution of low-volatility organics in the atmosphere. Atmos. Environ. 42, 3593–3624. https://doi.org/10.1016/j.atmosenv.2008.01.003

Kulmala, M., Pirjola, L., Mäkelä, J.M., 2000. Stable sulphate clusters as a source of new atmospheric particles. Nature 404, 66–69.

Kulmala, M., Maso, M.D., Makela, J.M., Pirjola, L., Vakeva, M., Aalto, P., Miikkulainen, P., Hameri, K., O'Dowd, C.D., 2001. On the formation, growth and composition of nucleation mode particles. Tellus B 53, 479–490.

Kulmala, M., 2003. How particules nucleate and grow. Science 302, AAC 15-1-AAC 15-6.

Kulmala, M., Vehkamäki, H., Petäjä, T., Dal Maso, M., Lauri, A., Kerminen, V.-M., Birmili, W., McMurry, P.H., 2004. Formation and growth rates of ultrafine atmospheric particles: a review of observations. J. Aerosol Sci. 35, 143–176.

Kulmala, M., Petäjä, T., Nieminen, T., Sipilä, M., Manninen, H.E., Lehtipalo, K., Dal Maso, M., Aalto, P.P., Junninen, H., Paasonen, P., Riipinen, I., Lehtinen, K.E.J., Laaksonen, A., Kerminen, V.-M., 2012. Measurement of the nucleation of atmospheric aerosol particles. Nat. Protoc. 7, 1651–1667.

Lee, S.-H., Young, L.-H., Benson, D.R., Suni, T., Kulmala, M., Junninen, H., Campos, T.L., Rogers, D.C., Jensen, J., 2008. Observations of nighttime new particle formation in the troposphere. J. Geophys. Res. 113, D10210.

Merikanto, J., Spracklen, D.V., Mann, G.W., Pickering, S.J., Carslaw, K.S., 2009. Impact of nucleation on global CCN. Atmos Chem Phys 16.

Mikkonen, S., Romakkaniemi, S., Smith, J.N., Korhonen, H., Petäjä, T., Plass-Duelmer, C., Boy, M., McMurry, P.H., Lehtinen, K.E.J., Joutsensaari, J., Hamed, A., Mauldin III, R.L., Birmili, W., Spindler, G., Arnold, F., Kulmala, M., Laaksonen, A., 2011. A statistical proxy for sulphuric acid concentration. Atmospheric Chem. Phys. 11, 11319–11334.

Ng, N.L., Kroll, J.H., Keywood, M.D., Bahreini, R., Varutbangkul, V., Flagan, R.C., Seinfeld, J.H., Lee, A., Goldstein, A.H., 2006. Contribution of First- versus Second-Generation Products to Secondary Organic Aerosols Formed in the Oxidation of Biogenic Hydrocarbons. Environ. Sci. Technol. 40, 2283–2297.

Nøjgaard, J.K., Nguyen, Q.T., Glasius, M., Sørensen, L.L., 2012. Nucleation and Aitken mode atmospheric particles in relation to O3 and NOX at semirural background in Denmark. Atmos. Environ. 49, 275–283.

Ortega, I.K., Suni, T., Boy, M., Grönholm, T., Manninen, H.E., Nieminen, T., Ehn, M., Junninen, H., Hakola, H., Hellén, H., Valmari, T., Arvela, H., Zegelin, S., Hughes, D., Kitchen, M., Cleugh, H., Worsnop, D.R., Kulmala, M., Kerminen, V.-M., 2012. New insights into nocturnal nucleation. Atmospheric Chem. Phys. 12, 4297–4312.

Paasonen, P., Nieminen, T., Asmi, E., Manninen, H.E., Petäjä, T., Plass-Dülmer, C., Flentje, H., Birmili, W., Wiedensohler, A., Hõrrak, U., Metzger, A., Hamed, A., Laaksonen, A., Facchini, M.C., Kerminen, V.-M., Kulmala, M., 2010. On the roles of sulphuric acid and low-volatility organic vapours in the initial steps of atmospheric new particle formation. Atmospheric Chem. Phys. 10, 11223–11242.

Pandis, S.N., Harley, R.A., Cass, G.R., Seinfeld, J.H., 1992. Secondary organic aerosol formation and transport. Atmospheric Environ. Part Gen. Top. 26, 2269–2282.

Peng, Y., Liu, X., Dai, J., Wang, Z., Dong, Z., Dong, Y., Chen, C., Li, X., Zhao, N., Fan, C., 2017. Aerosol size distribution and new particle formation events in the suburb of Xi'an, northwest China. Atmos. Environ. 153, 194–205.

Rose, C., Sellegri, K., Moreno, I., Velarde, F., Ramonet, M., Weinhold, K., Krejci, R., Andrade, M., Wiedensohler, A., Ginot, P., Laj, P., 2017. CCN production by new particle formation in the free troposphere. Atmospheric Chem. Phys. 17, 1529–1541.

RStudio Team (2016). RStudio: Integrated Development for R. RStudio, Inc., Boston, MA URL http://www.rstudio.com

Sandradewi, J., Prévôt, A.S.H., Szidat, S., Perron, N., Alfarra, M.R., Lanz, V.A., Weingartner, E., Baltensperger, U., 2008. Using Aerosol Light Absorption Measurements for the Quantitative Determination of Wood Burning and Traffic Emission Contributions to Particulate Matter. Environ. Sci. Technol. 42, 3316–3323.

Seinfeld, J.H., Pandis, S.N., 2006. Atmospheric chemistry and physics: from air pollution to climate change, 2nd ed. ed. J. Wiley, Hoboken, N.J.

Shen, X.J., Sun, J.Y., Zhang, Y.M., Wehner, B., Nowak, A., Tuch, T., Zhang, X.C., Wang, T.T., Zhou, H.G., Zhang, X.L., Dong, F., Birmili, W., Wiedensohler, A., 2011. First long-term study of particle number size distributions and new particle formation events of regional aerosol in the North China Plain. Atmospheric Chem. Phys. 11, 1565–1580.

Sipilä, M., Berndt, T., Petaja, T., Brus, D., Vanhanen, J., Stratmann, F., Patokoski, J., Mauldin, R.L., Hyvarinen, A.-P., Lihavainen, H., Kulmala, M., 2010. The Role of Sulfuric Acid in Atmospheric Nucleation. Science 327, 1243–1246.

Solomon, S., Intergovernmental Panel on Climate Change, Intergovernmental Panel on Climate Change (Eds.), 2007. Climate change 2007: the physical science basis: contribution of Working Group I to the Fourth Assessment Report of the Intergovernmental Panel on Climate Change. Cambridge University Press, Cambridge ; New York.

Stull, R.B., 1988. Mean Boundary Layer Characteristics, in: Stull, R.B. (Ed.), An Introduction to Boundary Layer Meteorology. Springer Netherlands, Dordrecht, pp. 1–27.

Uzu, G., Weber, S., Jaffrezo, J.-L., 2019. Pollution atmosphérique et impacts sanitaires. Colloq. Agric. Qual. Air 20.

Wagner, P., Schäfer, K., 2017. Influence of mixing layer height on air pollutant concentrations in an urban street canyon. Urban Clim. 22, 64–79.

Willeke, K., Baron, P.A. (Eds.), 1993. Aerosol measurement: principles, techniques, and applications. Van Nostrand Reinhold, New York.

Wu, Z., Hu, M., Liu, S., Wehner, B., Bauer, S., Ma ßling, A., Wiedensohler, A., Petäjä, T., Dal Maso, M., Kulmala, M., 2007. New particle formation in Beijing, China: Statistical analysis of a 1-year data set. J. Geophys. Res. 112, D09209.

Xiao, S., Wang, M.Y., Yao, L., Kulmala, M., Zhou, B., Yang, X., Chen, J.M., Wang, D.F., Fu, Q.Y., Worsnop, D.R., Wang, L., 2015. Strong atmospheric new particle formation in winter in urban Shanghai, China. Atmospheric Chem. Phys. 15, 1769–1781.

Yue, D.L., Hu, M., Zhang, R.Y., Wang, Z.B., Zheng, J., Wu, Z.J., Wiedensohler, A., He, L.Y., Huang, X.F., Zhu, T., 2010. The roles of sulfuric acid in new particle formation and growth in the mega-city of Beijing. Atmospheric Chem. Phys. 10, 4953–4960.

# Appendixes

# Appendix 1: R script for SMPS data

```
    ##This script computes particle number size distribution from SMPS--##
########## load packages to plot SMPS data ##########
    library(rlang)
library(smps)
library(varhandle)
library(dplyr)
library(tidyr)
library(data.table)
library(ggplot2)
library(scales) # for date_breaks
library(viridisLite)
library(grDevices)

    ########## load SMPS data set ##########
#first chose the working directory
WD = "C:/Users/lsimon/Desktop/LSIMON" #set the name of your WD
setwd(WD) # load it
    #choosing the dataset
ACSM_site <- "Grignon"
if (ACSM_site == "Grignon") {
  my_data <- read.csv("Data_SMPS_Grignon.csv", header = TRUE)
  } else {ACSM_site}
if (ACSM_site == "SIRTA") {
  my_data <- read.csv("Data_SMPS_SIRTA_corr.csv", header = TRUE)
  } else {ACSM_site}
    #my_data <- my_data[, -1]
setnames(my_data, old = "date", new="Time")
my_data$Time <- unfactor(my_data$Time)
my_data$Time <- as.POSIXct(strptime(my_data$Time, format = "%d/%m/%Y %H:%M", tz
= "UTC"))
    Diameter <- as.numeric(gsub("X", "", names(my_data)[-1])) # get the diameter of size
bins
Diameter_µm <- Diameter*10^-3
nb_size_bin <- ncol(my_data)

    #build a long dataframe
data_long <- gather(my_data, "Diameter", "dN_dlogDp", 2:nb_size_bin)
data_long$Diameter <- as.numeric(gsub("X", "", data_long$Diameter )) # set diameter as a
numeric
# we want time as a date-formatted variable
x <- as.character(data_long$Time)
date_ <- gsub(" ", "", substr(x, 1, nchar(x)-8))
time_ <- gsub(" ", "", substr(x, nchar(x) - 4, nchar(x)))
data_long$Time <- x

    #calculate the log value of dNdlogDp
data_long$dN_dlogDp_log <- log10(data_long$dN_dlogDp)
data_long$dN_dlogDp_log <- ifelse(data_long$dN_dlogDp_log == "NaN" |
                            data_long$dN_dlogDp_log == "-Inf"  , 0.01,
data_long$dN_dlogDp_log)
```

```
#filter NA and infinite data
data_long[is.na(data_long)] <- 0.01
data_long[is.infinite(data_long$dN_dlogDp_log)] <- 0.01
data_long[is.infinite(data_long$dN_dlogDp)] <- 0.01
# interpolate between the  values for a smoother contour
# this takes a moment or two...
# increase these values to make it quicker, trial and error!
# get on with plotting: make log and raw data into a data frame for ggplot
    data_long_log <- data_long[,c(1,2,4)]
data_long_raw <- data_long[,c(1,2,3)]

    ########################## plots #####################################
    # function for minor tick marks
every_nth <- function(x, nth, empty = TRUE, inverse = FALSE)
{
 if (!inverse) {
   if(empty) {
     x[1:nth == 1] <- ""
     x
   } else {
     x[1:nth != 1]
   }
 } else {
   if(empty) {
     x[1:nth != 1] <- ""
     x
     } else {
     x[1:nth == 1]
   }
 }
}
    # get visually diminishing axis ticks
base_breaks <- function(n = 10){
 function(x) {
   axisTicks(log10(range(x, na.rm = TRUE)), log = TRUE, n = n)
 }
}
    insert_minor <- function(major_labs, n_minor) {labs <-
 c( sapply( major_labs, function(x) c(x, rep("", multiple) ) ) )
labs[1:(length(labs)-n_minor)]}
    # adjust the colour ramp to match the Igor plot, please experiment with the numbers here!
colfunc <- colorRampPalette(c( rep("red", 3),
                        rep("yellow", 1),
                        rep("green", 1),
                        "cyan",
                        rep("blue", 3),
                        "purple"))
    # function to set the legend labels
fill_scale_labels <- function(x) {
 parse(text = paste0("10^",x))
}
```

```
    y_labels_breaks <- seq(0, max(Diameter), 10)
mytheme <- theme_bw(base_size = 14) +  theme(aspect.ratio = 1.6/5)
    mytheme2 <- theme(plot.title = element_text(face="bold.italic")) +
  theme(legend.title = element_text(size=10)) +
  theme(legend.text = element_text(size=10)) +
  theme(axis.title.x = element_text(size=10)) +
  theme(axis.title.y = element_text(size=10))

    ## Make banana plots ##
    # add tick marks every X hours
start_date <- as.POSIXct(data_long_log$Time[1],tz="UTC", format = "%Y-%m-%d
%H:%M:%S")
end_date <-  as.POSIXct(data_long_log$Time[nrow(data_long_log)],tz="UTC", format =
"%Y-%m-%d %H:%M:%S")
date_breaks_6h <-  seq(from = start_date, to = end_date, by = "6 hours")
date_breaks_1_day <- seq(from = start_date, to = end_date, by = "1 day")
multiple <- length(date_breaks_6h) / length(date_breaks_1_day)
    #reformat time in POSIXct
data_long_log$Time <- as.POSIXct(data_long_log$Time,tz="UTC", format = "%Y-%m-%d
%H:%M:%S")
data_long_raw$Time <- as.POSIXct(data_long_raw$Time,tz="UTC", format = "%Y-%m-%d
%H:%M:%S")
    #Banana for log data (recommended)
# Now with log axis, we need to replace the ymin and ymax
distance <- diff((unique(data_long_log$Diameter)))/2
upper <- (unique(data_long_log$Diameter)) + c(distance, distance[length(distance)])
lower <- (unique(data_long_log$Diameter)) - c(distance[1], distance)
    # Create xmin, xmax, ymin, ymax
data_long_log$xmin <- data_long_log$Time - 1000 # default of geom_raster is 0.5
data_long_log$xmax <- data_long_log$Time + 1000
idx <- rle(data_long_log$Diameter)$lengths[1]
data_long_log$ymin <- unlist(lapply(lower, function(i) rep(i, idx)))
data_long_log$ymax <- unlist(lapply(upper, function(i) rep(i, idx)))
    ## THE LOOP ##
## careful takes some time to plot all data
    pdf(file = "SMPS_Grignon.pdf")
    First_day <- as.POSIXct(min(date_), tz = "UTC")
Last_day <-  as.POSIXct(max(date_), tz = "UTC") #as.POSIXct(max(date_), tz = "UTC")
Days <- seq.Date(as.Date(First_day), as.Date(Last_day), by="day")
Nb_of_days <- length(Days)
    for (i in 1:length(Days)) {
Day_to_plot <- as.character(Days[i], format("%Y-%m-%d"))
 one_day <- data_long_log[grepl(Day_to_plot, data_long_log$Time), ] #get the data
corresponding to the selected day
 one_day <- data_long_log %>%
   filter(grepl(Day_to_plot, Time)) #filter data
      start_date <- min(one_day$Time)
  end_date <-  max(one_day$Time)
      time_labels_breaks <- seq(start_date, end_date, "4 hours") # add grah x labels every
XXX hours
  time_labels_breaks <- as.POSIXct(time_labels_breaks, tz="UTC")
```

```
    print(ggplot(data_long_log, aes(y = Diameter, x = Time,
                      xmin=xmin, xmax=xmax, ymin=ymin, ymax=ymax,
                      fill = dN_dlogDp_log)) +
  geom_rect()  +
  scale_fill_gradientn(name=expression(dN/dlogD[p](cm^-3)),
                       colours = rev(colfunc(100)),
                       labels = fill_scale_labels,
                       limits=c(0, 5.5))  +
  scale_y_continuous(expand = c(0,0),
                     limits = c(4,160),
                     trans = log_trans(), breaks = base_breaks()) +
  scale_x_datetime(expand = c(0,0),
                   limits = c(as.POSIXct(start_date, tz="UTC"), as.POSIXct(end_date, tz="UTC")),
                   breaks = time_labels_breaks,
                   labels = strftime(time_labels_breaks, "%H:%S", tz="UTC"))  +
  xlab("Time") +
  ylab("Diameter (nm)") +
  ggtitle(paste(Day_to_plot)) +
  mytheme +
  mytheme2)
}
    dev.off()
```

## Appendix 2: R script to calculate growth rates

```
    #choose working directory
WD = "C:/Users/lsimon/Desktop/LSIMON/SMPS/Growth rate"
setwd(WD)
    #define time step between each point
time_step <- (5/60) #in hour
dir.create("sortiesR")
    #load diameters file
diameters <- read.csv("Data/Diameters.csv", header = FALSE)
    #make list of NPF days files in a folder
list_of_events <- list.files(paste0(WD,"/Data"))
list_of_events <- list_of_events[-grep("Diameter",list_of_events)]
    #define function to find modes
find_modes<- function(x) {
 modes <- NULL
 for (i in 4:(length(x)-3)){
  if ((x[i] > max(x[i-3], x[i-1]) & (x[i] > max(x[i+1], x[i+3])) )) {
   modes <- c(modes,i)
  }
 }
 if ( length(modes) == 0 ) {
  modes = 'This is a monotonic distribution'
 }
 return(modes)
}
    for (i in list_of_events) {
 i <- list_of_events[2]
    #read dN file and change date format
file_to_read <- paste0("Data/",i)
dN <- read.csv(file_to_read, header = FALSE)
dN$V1 <- unfactor(dN$V1)
dN$V1 <- as.POSIXct(dN$V1, format = "%m/%d/%Y %H:%M", tz = "UTC")
setnames(dN, old = "V1", new="date")
dN <- dN[complete.cases(dN), ]
    #create path and pdf file for each NPF day
Event_date <- substr(i,1,10)
dir_to_create <- paste0("sortiesR/",Event_date)
dir.create(dir_to_create)
PDF_name <- paste0(dir_to_create, "/", Event_date, ".pdf")
pdf(PDF_name)
    df_mode_1 <- NULL
    for (j in 1:nrow(dN)){
my_data <- data.frame(diameters[, 1], as.numeric(dN[j,-1]))
colnames(my_data) <- c("diameters", "dN")
    my_data$index <- 1:nrow(my_data)
#smooth dN values
loessMod50 <- loess(dN ~ index, data=my_data, span=0.50) # 50% smoothing span
smoothed50 <- predict(loessMod50)
write.csv(smoothed50, paste0(dir_to_create, "/", "smoothed50.csv"))
    #find modes in the smoothed values to select highest value (mode indice)
mymodes_indices <- find_modes(smoothed50)
```

```
mymodes_diam <- my_data$diameters[mymodes_indices]
mymodes_dN <- my_data$dN[mymodes_indices]
    #keep only first mode indice (finest particles)
mode_1 <- data.frame(dN[j,1], mymodes_diam[1])
colnames(mode_1) <- c("date", "mode_diameter")
mode_1 <- mode_1[complete.cases(mode_1), ]
df_mode_1 <- rbind(df_mode_1, mode_1)
colnames(df_mode_1) <- colnames(mode_1)
    #plot dN values and smoothed (line)
plot(my_data$diameters, my_data$dN, log = "x", main = paste(dN$date[j]), xlab = "diameter
(nm)", ylab = "dN") + lines(my_data$diameters, smoothed50, col = "blue")
}
    for (k in 2:nrow(df_mode_1)) {
 if(df_mode_1$mode_diameter[k] < 50) {
 } else {
  df_mode_1$mode_diameter[k] <- df_mode_1$mode_diameter[k-1]
 }
}
write.csv(df_mode_1, paste0(dir_to_create, "/", "dataframe_first_mode.csv"))
dev.off()
    df_mode_1$growth_rate <- 0
    #smooth values for growth rates
df_mode_1$index <- seq(1:nrow(df_mode_1))
loessMod50_gr <- loess(mode_diameter ~ index, data=df_mode_1, span=0.50) # 50%
smoothing span
smoothed50_gr <- predict(loessMod50_gr)
pdf(paste0(dir_to_create, "/","first_mode.pdf"))
plot(df_mode_1$date, smoothed50_gr)
    write.csv(df_mode_1)
dev.off()
    #calculate growth rate
for (l in 1:nrow(df_mode_1)) {
 df_mode_1$growth_rate[l] <- (smoothed50_gr[l+1]-smoothed50_gr[l])/time_step
}
    pdf(paste0(dir_to_create, "/", "growth_plot_", Event_date, ".pdf"))
plot(df_mode_1$date,df_mode_1$growth_rate, main="Growth rate", xlab="Time", ylab="GR
(nm/h)")
dev.off()
write.csv(cbind(as.POSIXct(df_mode_1$date, format = "%Y-%m-%d %H:%M", tz =
"UTC"), df_mode_1$growth_rate), paste0(dir_to_create, "/growth_rate_", Event_date,
".csv"))
}
```

# Appendix 3: All daily number size distribution

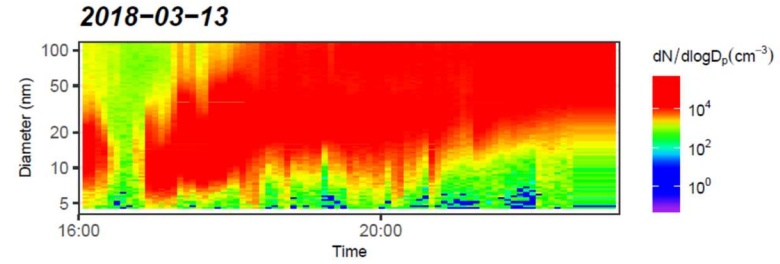


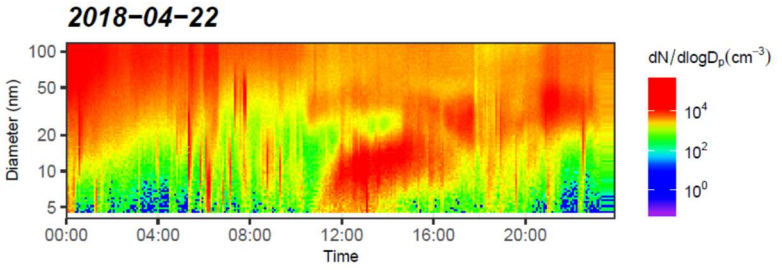


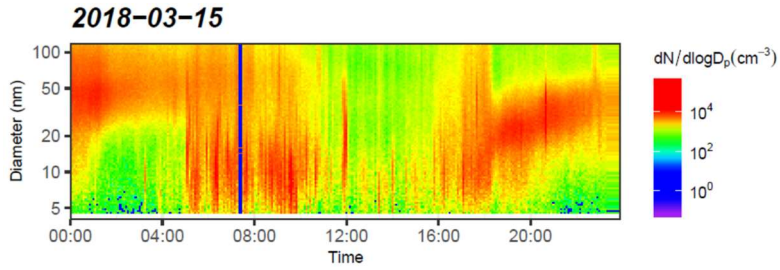


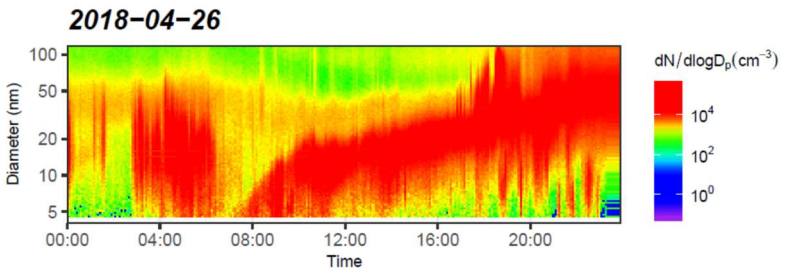


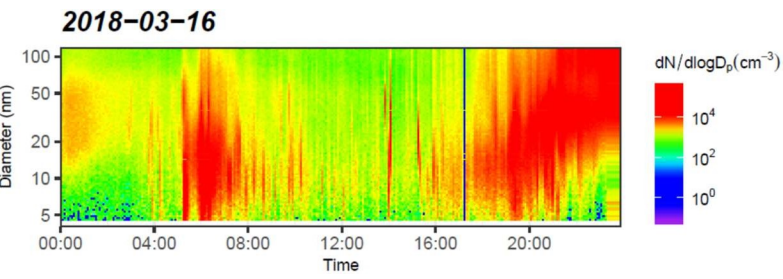


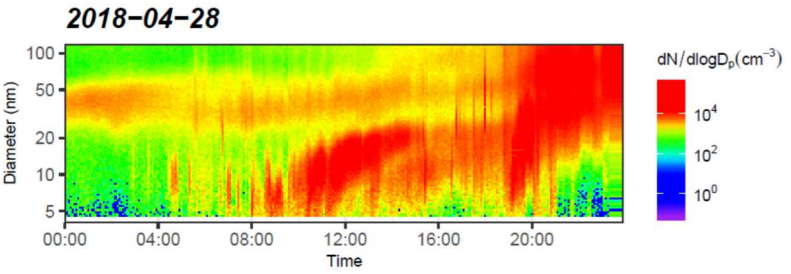


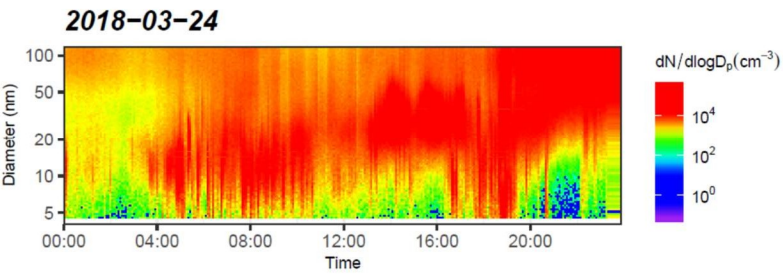


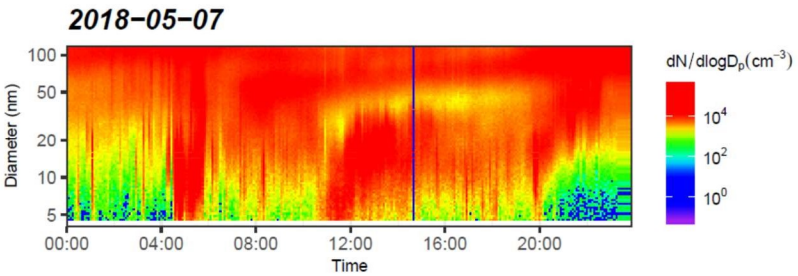


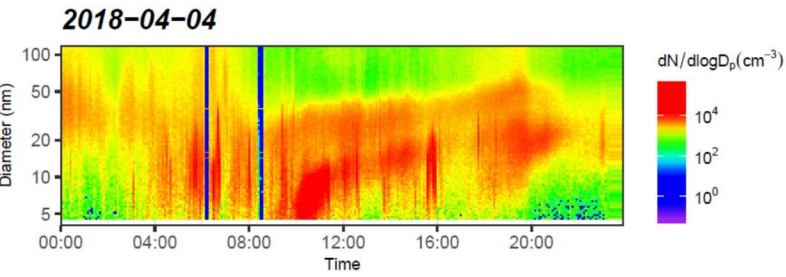


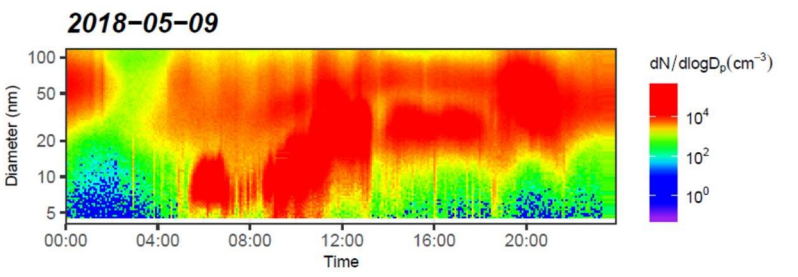


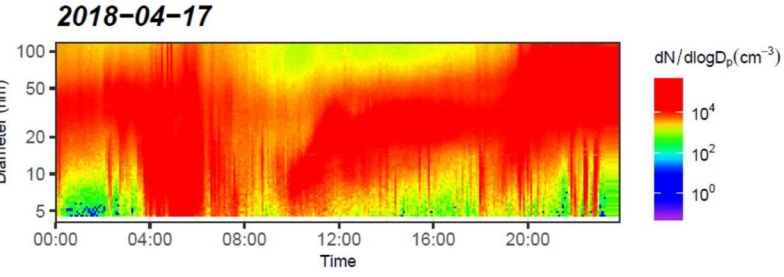


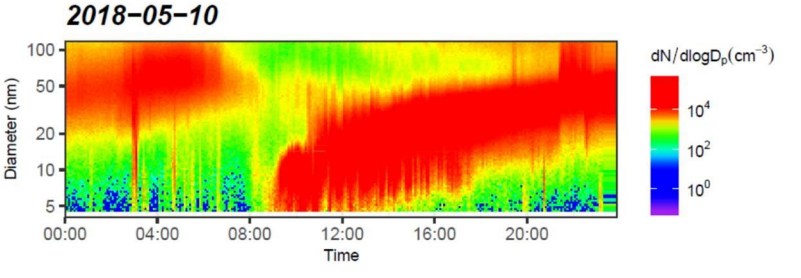

# Appendix 4: All diurnal profiles

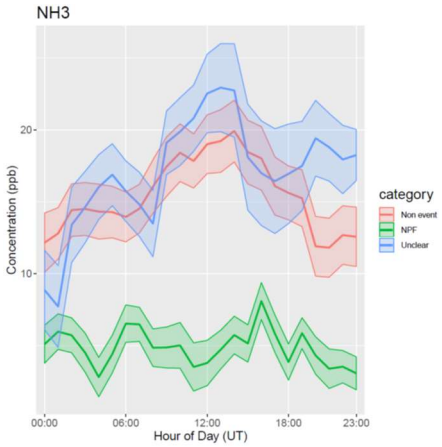


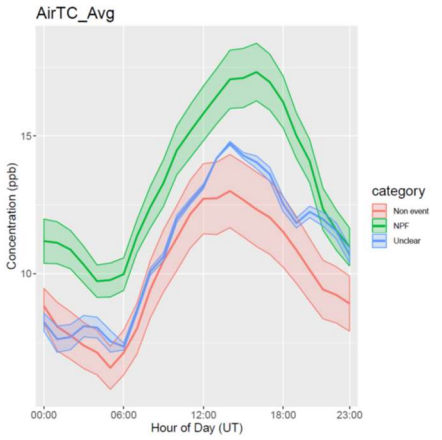


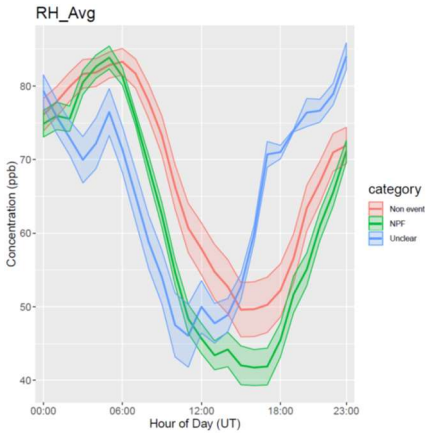


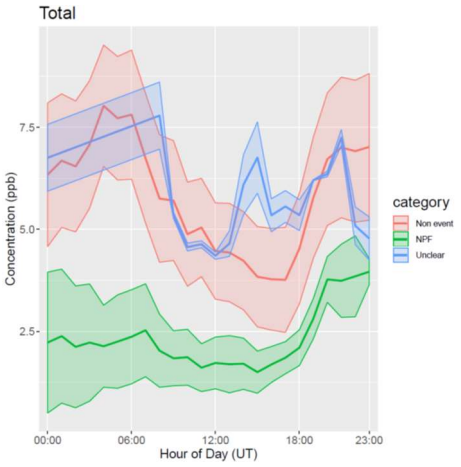


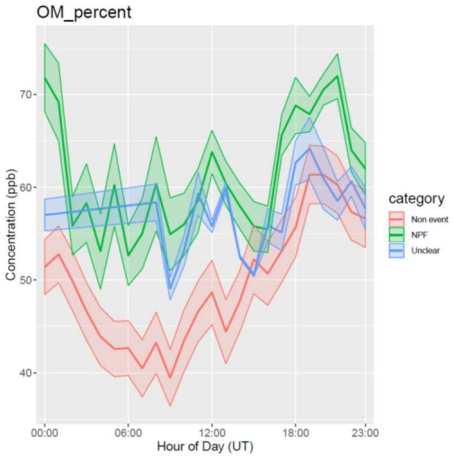


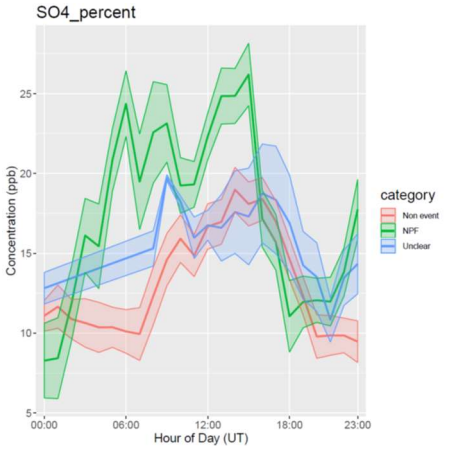


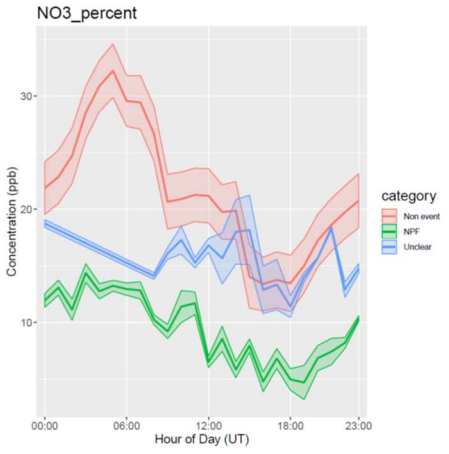


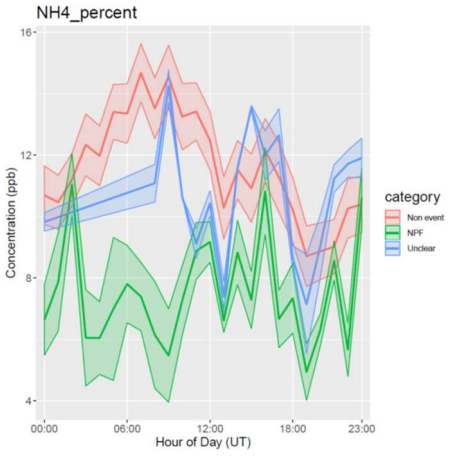


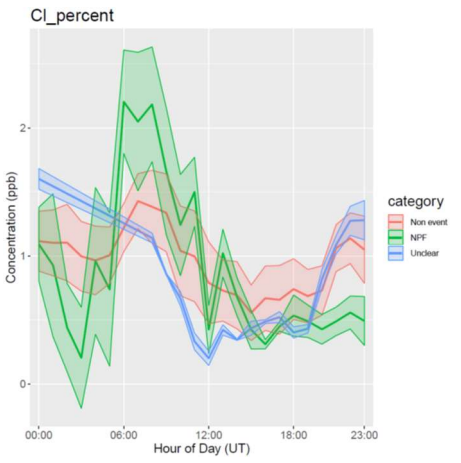


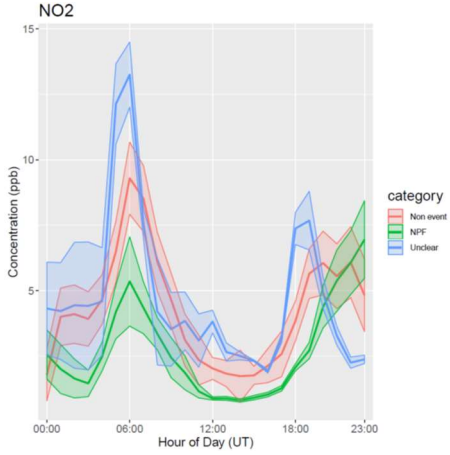


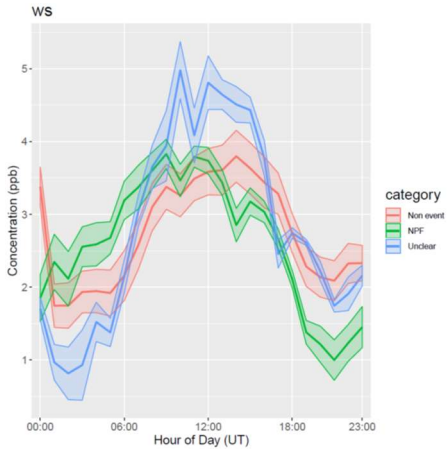


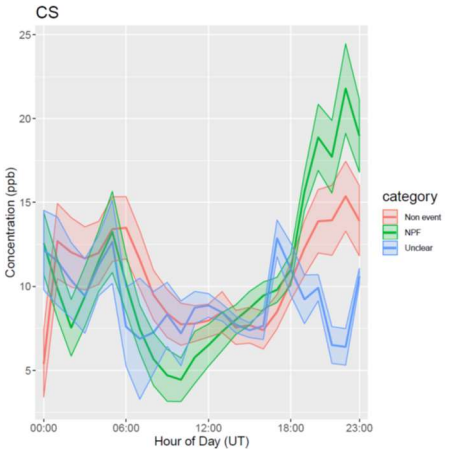

# Appendix 5: Time series of daytime NPF events and parameters

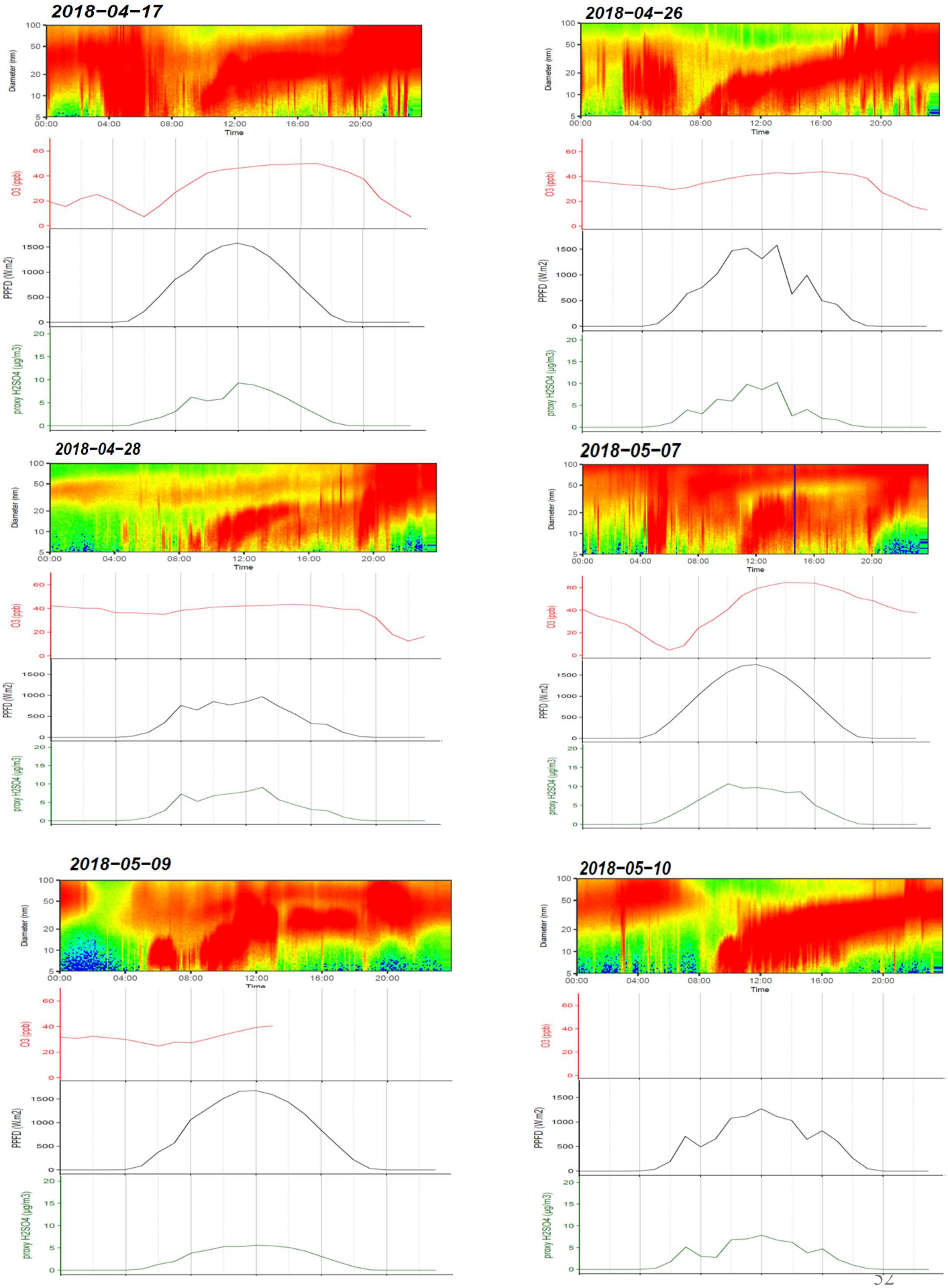

# Appendix 6: All nocturnal profiles

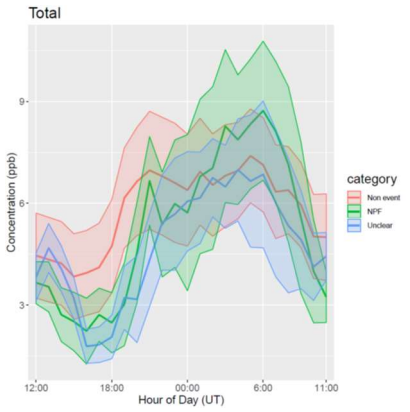


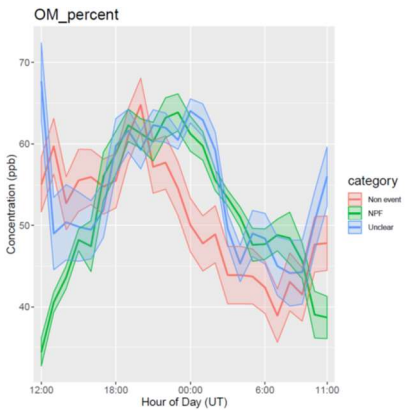


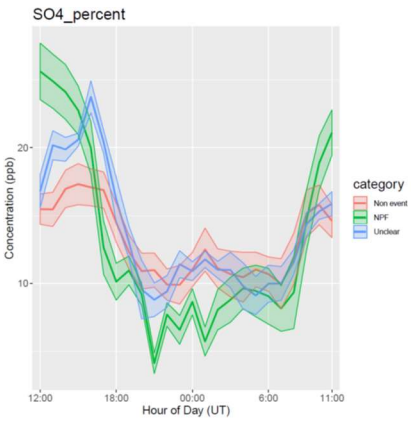


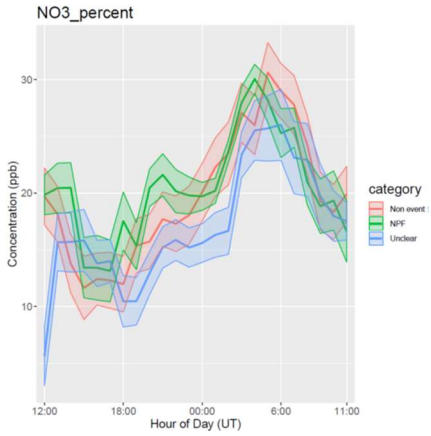


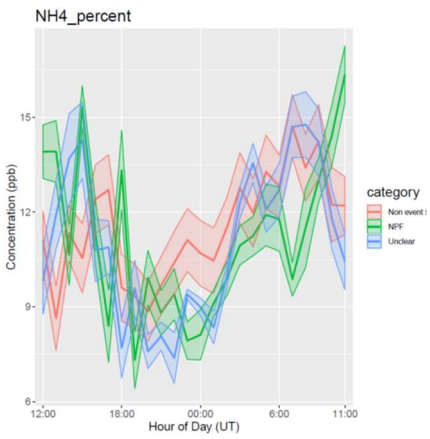


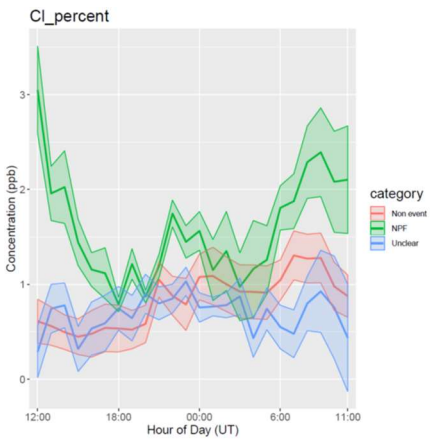


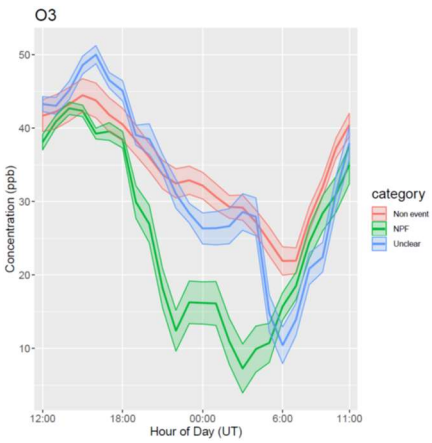


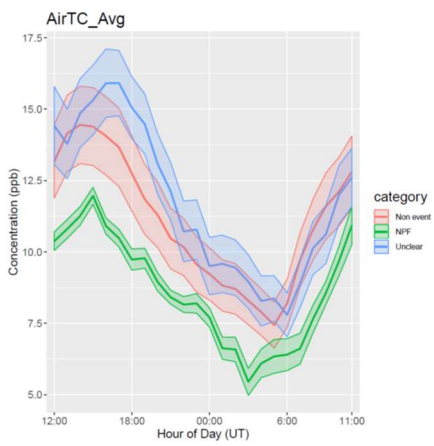


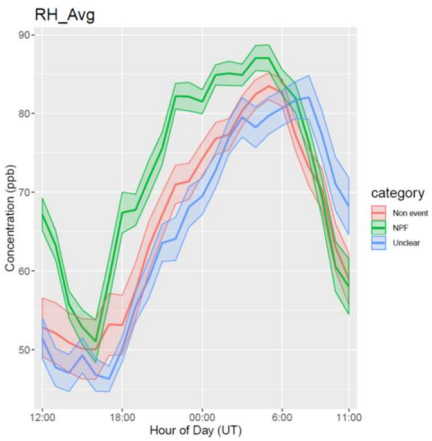


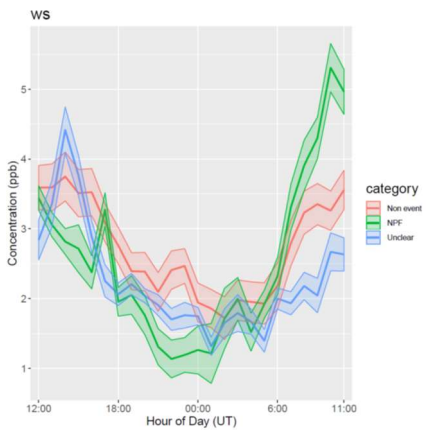


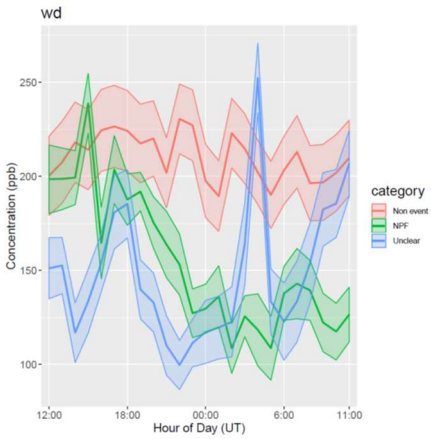


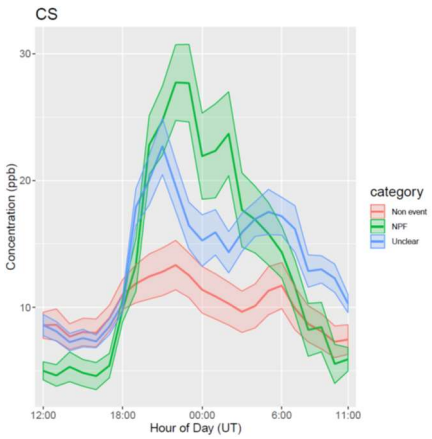

MASTER'S DEGREEE
Chemistry
Specialty : **« Environmental Sciences and Engineering »**

| | |
|---|---|
| YEAR: 2017-2019 | PRESENTATION DATE: September, 18th, 2019 |
| AUTHOR: Leïla SIMON | INTERNSHIP LOCATION: LSCE |
| UNIVERSITY SUPERVISOR: Maxime PONTIE | COMPANY SUPERVISOR: Jean-Eudes PETIT |

TITLE:
NEW PARTICLE FORMATION IN AN AGRICULTURAL ENVIRONMENT

KEYWORDS: New Particle Formation, agriculture, atmospheric aerosols, nucleation, growth

ABSTRACT:

The understanding of sources and formation mechanisms of particulate pollution represents a major challenge on both scientific and social levels, through sanitary and climatic impacts. The Ile-de-France region is particularly affected by episodes of particulate pollution which are often related, during spring, to agricultural activities. However, while primary emissions are quite well documented, the agricultural ecosystem is still scarcely studied in terms of new particle formation (NPF). This process corresponds to the formation of a particulate nucleus followed by their growth, by gas-particle conversion of semi-volatile compounds. While NPF has already been observed in numerous locations, very few studies were conducted in the agricultural field.

As part of the ADEME-AgriMultiPol project, a field campaign took place on the FR-Gri ICOS site in the Grignon experimental farm, from March 13th to May 14th 2018. In order to identify new particle formation events, measurements of the particle number size distribution were carried out. Complementary analyses of chemical characterization of the particles, meteorological parameters and gas concentration have been performed to investigate the origin of NPF.

This unique dataset in the vicinity of agricultural activities enabled firstly to identify diurnal and nocturnal new particle formation events. Secondly, linking the events with the environmental parameters highlighted conditions and interesting tendencies. It was shown that the diurnal events could be linked to the photooxidation of precursor VOCs, while the nocturnal events seemed to be favoured by the presence of nitrogen dioxide and ammonia.

Finally, a comparison with measurements at the SIRTA station, 27 km away, showed that these events occurred on a regional scale, as they happened almost simultaneously at both sites.

RESUME:

La compréhension des sources et des mécanismes de formation de la pollution particulaire représente un enjeu majeur aux niveaux scientifique et sociétal, au travers d'impacts sanitaires et climatiques. L'Ile de France est particulièrement touchée par des épisodes de pollution particulaire auxquels, au printemps, l'agriculture est souvent associée. Pourtant, alors que les émissions primaires sont de mieux en mieux documentées, l'écosystème agricole reste assez peu étudié au regard de la formation de nouvelles particules (NPF). Ce processus correspond à la formation d'un noyau particulaire suivi d'un grossissement, par conversion gaz-particule de composés semi-volatils. S'il a déjà été mis en évidence dans de nombreuses localisations, il n'existe que très peu d'études en milieu agricole.

Dans le cadre du projet AgriMultiPol, une campagne de mesures a été effectuée sur le site FR-Gri ICOS à la ferme expérimentale de Grignon, sur la période du 13 mars au 14 mai 2018. Afin d'identifier des épisodes de formation de nouvelles particules, des mesures de distribution granulométrique des particules ont été effectuées. Des mesures complémentaires de caractérisation chimique des particules, paramètres météorologiques et concentration en composés gazeux ont été mises en place pour étudier l'origine des NPF.

Ce jeu de données en proximité agricole, unique en son genre, a permis dans un premier temps de mettre en évidence des épisodes de formation de nouvelles particules diurnes et nocturnes. Dans un deuxième temps, le croisement des données a rendu possible la mise en relation de ces épisodes avec les conditions environnementales du site. Il a notamment été montré que les épisodes diurnes pouvaient être liés à la photooxidation de COVs précurseurs, tandis que les épisodes nocturnes semblent être favorisés par la présence de dioxyde d'azote et d'ammoniac.

Enfin, une comparaison avec les mesures effectuées à la station du SIRTA, située à 27 km de Grignon, montre que ces processus se déroulent à l'échelle régionale, car ils ont lieu de manière quasi simultané sur les deux sites.

Je soussigné Jean-Eudes PETIT maître de stage professionnel de Leïla SIMON,
AUTORISE ~~ou N'AUTORISE PAS~~ (1) : la publication des sources bibliographiques, des résumés français, anglais
AUTORISE ~~ou N'AUTORISE PAS~~ (1) : le dépôt du mémoire dans une bibliothèque
Date : 02/09/2019 Signature du maître de stage :



(1) rayer la mention inutile